2014

Entangled Photon Pairs in Disordered Photonic Lattices

Lane Martin
University of Central Florida

ENTANGLED PHOTON PAIRS IN DISORDERED PHOTONIC LATTICES

by

LANE A. MARTIN
B.S. Missouri University of Science and Technology, 2009

A dissertation submitted in partial fulfilment of the requirements
for the degree of Doctorate of Philosophy
in the College of Optics and Photonics
at the University of Central Florida
Orlando, Florida

Fall Term
2014

Major Professor: Bahaa E.A. Saleh

ABSTRACT

Photonic lattices consisting of arrays of evanescently coupled waveguides fabricated with precisely controlled parameters have enabled the study of discrete optical phenomena, both classical and quantum, and the simulation of other physical phenomena governed by the same dynamics. In this dissertation, I have experimentally demonstrated transverse Anderson localization of classical light in arrays with off-diagonal coupling disorder and investigated theoretically and experimentally the propagation of entangled photon pairs through such disordered systems. I discovered a new phenomenon, Anderson co-localization, in which a spatially entangled photon pair in a correlated transversally extended state localizes in the correlation space, though neither photon localizes on its own. When the photons of a pair are in an anti-correlated state, they maintain their anti-correlation upon transmission through the disordered lattice, exhibiting Anderson anti-localization. These states were generated by use of parametric down conversion in a nonlinear crystal. The transition between the correlated and anti-correlated states was also explored by using a lens system in a configuration intermediate between imaging and Fourier transforming. In the course of this research, I discovered a curious aspect of light transmission through such disordered discrete lattices. An excitation wave of a single spatial frequency (transverse momentum) is transmitted through the system and is accompanied by another wave with the same spatial frequency but opposite sign, indicating some form of internal reflection facilitated by the disordered structure.

Dedicated to my wife Lauren and the rest of my family, for putting up with me.

ACKNOWLEDGMENTS

I would like to acknowledge the group of advisors, colleagues, and confidants who have made my experiences at CREOL so valuable. My co-advisor, Dr. Abouraddy, has provided excellent guidance and support and has been instrumental in advancing my understanding of my own research and quantum optics as a whole. Gianni Giuseppe's help was critical to all my experimental efforts and his mentorship was a valued part of my graduate career. Kumel Kagalwala, my lab mate, has been a constant friend and respected colleague.

I would also like to acknowledge Dr. Christodoulides and his research group at CREOL for their significant contributions to my research, as well as Dr. Szameit and his research group in Jena, Germany, who provided the photonic lattices and without whom this research would not have been possible.

Finally I acknowledge my advisor, Dr. Saleh, for his support, guidance, insight, patience and wisdom. I will never forget the profound and incredible opportunity he has given me to pursue and learn about optics, physics and science. It has been an experience for which I am truly and eternally grateful.

TABLE OF CONTENTS

LIST OF FIGURES

CHAPTER 1: INTRODUCTION

Discrete optics is the study of light confined to networks of guiding structures such as fibers or waveguides. In such systems, the electric field evolves according to a set of discretized equations, the parameters of which depend on the specifics of the optical system. Here, I present the research I have performed and published on light propagation in photonic lattices in both the classical and quantum regimes. These papers discuss disordered photonic lattices and the onset of transverse Anderson localization with classical light and quantum entanglement of photon pairs evolving in disordered lattices. I reveal the related phenomena of Anderson co-localization and anti-localization, in which an entangled photon pair traversing a disordered photonic lattice localizes in correlation space, though neither photon localizes on its own. Additionally, I demonstrate a gradual transition between these two phenomena. I conclude with an experiment that explores effects related to the phase or spatial frequency of light propagating in these devices.

In 1935 Einstein, Podolsky and Rosen published a paper questioning the completeness of the quantum mechanical description of reality [1]. They proposed an experiment demonstrating that two particles that interacted at some time in the past could possess correlations that appeared to violate the laws of relativity laid down by Einstein years earlier. The EPR paradox, as it came to be known, was resolved by John S. Bell in 1964 [2]. The notion of entanglement crystallized in the following decades, followed by an era of experiment and discovery that continues today. Entanglement between two particles occurs when the state of the particles is no longer separable. In layman's terms, this means that neither particle can be completely described without referencing the other. This means that a measurement made on one particle, determining its state, yields immediate knowledge of the state of the other particle, collapsing its wave function. This occurs instantaneously, even if the particles are separated by large distances. Causality is preserved, however, as no information can be conveyed only by these means. Entanglement is now recognized as one of the most

counterintuitive and potentially useful phenomena in modern physics. It is a source of rich physics [3] and enables technologies beyond the bounds of classical physics, such as secure encryption [4, 5] and quantum computation [6].

Photonic waveguide lattices are integrated, multiport optical interferometers. They consist of evansescently coupled waveguides, which allows light propagating in one waveguide to couple to other nearby waveguides. These devices have generated significant interest, as their customizablility and inherent stability have enabled a variety of experiments that are not practical with bulk optical systems. These devices can be created such that light propagating in them mimics other types of particles; one their first uses was to demonstrate and study transverse Anderson localization (AL) [7, 8, 9, 10, 11, 12], a phenomenon native to condensed matter physics [13]. In its original context, Anderson localization occurs when an electron evolves on a disordered atomic lattice in the tight binding approximation. In a perfectly periodic lattice, the electron wavefunction evolves ballistically, traversing the lattice. Once disorder is introduced, perhaps affecting the probability of hopping between atoms, multiple scattering events serve to localize the electron on its initial site. In this way, disorder in the system serves to suppress diffusion, rather than enhancing it. While this effect has proven difficult to observe in its original context, it is readily realized in photonic lattices, where the electric field of light mimics the evolution of the electron wave function and the z-direction of the lattice takes on the role of time. As detailed in our research [9], averaging over multiple realizations of disorder reveals the exponential localization signature, centered on the input waveguide. This is the subject of the paper in Chapter 2 of this dissertation, where we demonstrate and detail Anderson localization of light in photonic lattices endowed with off-diagonal disorder [9].

Once AL has been observed for classical light in photonic lattices, the natural next step is to examine the evolution light with non-classical properties in such systems. In my research, I explored in both theory and experiment how spatially entangled photon pairs evolved in array with and with-

out off-diagonal disorder [14]. In the first of these experiments, detailed in Chapter 3, I coupled strongly correlated entangled photon pairs into periodic and disordered arrays and measured the spatial correlations of the emerging photons. I did this for both separable and entangled states. For the separable states, I recorded a second order correlation function $G^{(2)}(x_1, x_2)$ with the same form as classical AL for both periodic and disordered arrays, as expected. I then coupled into the array entangled photon pairs such that the photons will always enter the same waveguide, though which waveguide among those illuminated is unknown. In the periodic case, I observed the ballistic expansion of the input state, but oriented along the $x_1 = x_2$ axis. For the disordered arrays, I observed a new phenomenon termed Anderson co-localization, in which neither photon localizes on its own (due to the broad spatial extent of the input state) but the photons do localize in correlation space along the $x_1 = x_2$ axis, meaning the photons emerge from the same or nearby waveguides. In this paradigm, the entangled photons retained their spatial correlations, even after propagation through a highly disordered discrete medium.

In the next paper [15], I expanded upon my previous research and explored the action of the disordered array with input states in which the entanglement was expressed in different ways. First, I used an anti-correlated two photon entangled input state. Here, the two photons enter the photonic lattice on opposite sides of a central waveguide ($x_1 + x_2 =$ Const.). With this input state, we observed the phenomenon of Anderson anti-localization (AaL). Once again, the photons retain the spatial correlations present in the input state; now the emerging photons are anti-localized, concentrated along the $x_1 = -x_2$ axis of the function $G^{(2)}(x_1, x_2)$. In addition, I utilize so-called intermediate input states, in which the photons are neither stongly localized or anti-localized. Knowledge of the position of one photon yields a range of positions for the other. I note that the photons are still entangled, but the entanglement is expressed in the phase (or spatial frequency) correlations between the photons, not their position. We implement these intermediate states via a fractional Fourier transforming input optical system, altering it so as to cause a transition between the anti-

correlated and correlated input states. I predicted and experimentally measure this transition before and after the array, showing how the spatial correlations are preserved by the array.

In the final paper, I examine the action of the arrays in terms of the spatial frequency of an input electric field. Photonic waveguide arrays have been extensively studied in the classical and quantum regimes, yet little research has been done on how even the simplest arrays affect the spatial frequency spectrum. We address this question for periodic and disordered arrays by simulating and experimentally measuring the magnitude square of the impulse response functions in the spatial and spatial frequency coordinates. I begin with a review of the theory describing the evolution of the electric field in one dimensional waveguide arrays and show how it can be reinterpreted in terms of spatial frequency. I then show how the various impulse response functions, or their approximations, can be experimentally measured. For the periodic array, I show the detailed structure generated by observing a spatial frequency output with a spatial impulse input and explain its origin. In the disordered array, I found that, surprisingly, a spatial frequency impulse input state is not obscured by the high level of disorder in the array; instead it is split into two components with opposing spatial frequencies, akin to transmitted and reflected components. This result is perhaps unexpected, and reinforces the dramatic difference between continuous and discrete optical systems.

CHAPTER 2: TRANSVERSE ANDERSON LOCALIZATION WITH CLASSICAL LIGHT

Introductory Remarks on Experiment One

The following paper was originally published in Optics Express [9]. It details research I performed using photonic lattices injected with classical light, in which we show transverse Anderson localization of light after shifting the array and averaging the output. This paper begins with a discussion of the equations that govern the propagation of light in waveguide arrays, followed by numerical simulations of the results and discussion of the experimental setup. We observe the light to be, on average, exponentially localized on the input waveguide and verify that the approach of shifting and averaging on the same array yields the same results as averaging over multiple independent realizations of disorder.

This experiment serves to characterize the periodic and disordered arrays using classical light, and to serve as a starting point for understanding the action of the arrays on more complicated states of light. We show conclusively that these devices induce Anderson localization through both experiment and numerical simulation.

Anderson Localization in Optical Waveguide Arrays with Off-Diagonal Coupling Disorder

L. Martin, G. Di Giuseppe, A. Perez-Leija, R. Keil, F. Dreisow, M. Heinrich, S. Nolte, A. Szameit, A.F. Abouraddy, D.N. Christodoulides and B.E.A. Saleh, Optics Express, 19, 13636, 2011.

Abstract

We report on the observation of Anderson wave localization in one-dimensional waveguide arrays with off-diagonal disorder. The waveguide elements are inscribed in silica glass, and a uniform random distribution of coupling parameters is achieved by a precise variation of the relative waveguide positions. In the absence of disorder we observe ballistic transport as expected from discrete diffraction in periodic arrays. When off-diagonal disorder is deliberately introduced into the array we observe Anderson localization. The strength of the localization signature increases with higher levels of disorder.

Introduction

Anderson localization is ubiquitous in wave physics. This process naturally arises in any random lattice system and is known to result from the interference between multiple scattering events. Under strong disorder conditions this interference can become so severe that it entirely holds the transport of a quantum mechanical wave-packet. In this regime, Anderson localization occurs. While in higher dimensions the transition from ballistic to Anderson localization is preceded by diffusion, in 1D-systems this effect can be directly induced even in the presence of weak disorder [13, 10]. Over the years Anderson localization has been analyzed in the literature under both diagonal [13] and off-diagonal disorder conditions [16, 17].

Lattices of coupled optical waveguides provide a versatile platform for manipulating the flow of light [18]. In recent years such arrays have been used to directly observe and study optical analogs of many fundamental quantum mechanical effects like Bloch oscillations [19, 20] , Zener tunneling [21], continuous-time quantum random walks [22], and other processes [23, 24, 25]. Another example is Anderson localization that has been directly observed for light propagating in one- (1D) and two-dimensional (2D) arrays of coupled waveguides [11, 12]. These observations have been demonstrated for the case of diagonal disorder, i.e., the waveguide propagation constants are randomized (by randomizing the sizes of the waveguides), while keeping the coupling coefficients between adjacent waveguides approximately constant (by keeping the waveguide separations constant). Anderson localization for off-diagonal disordered waveguide arrays has been reported for the first time in Ref. [26]. In such an array, the waveguide elements are all identical (i.e. have the same propagation constant) while the coupling coefficients are varied by changing their relative positions. In Ref. [26], disorder-induced localization by averaging over many array samples having the same degree of disorder was observed in 1D photonic lattices. We report here the observation of Anderson localization in a 1D optical waveguide array with off-diagonal disorder having a uniform random distribution of coupling coefficients. We prove through experimental observation and calculation that the shift invariance of the statistical characteristics of the waveguide disorder allows one to replace statistical averaging over multiple sample realizations with shifting the input waveguide excited in the same sample realization. Furthermore, we examine the effect of the waveguide array length on the propagation dynamics in both the periodic and the disordered arrays.We would like to emphasize that while both diagonal and off-diagonal disorder can lead to Anderson localization, there are still qualitative differences between them [27]. One such aspect manifests itself in the level of disorder needed to accomplish 1D localization. In general, for off-diagonal disorder, stronger level of randomness is necessary compared to that required for diagonal disorder if the same localization length is to be attained. Reference [28] highlights this issue among other distinguishing traits of off-diagonal disorder.

The waveguides used here are fabricated by use of intense infrared femtosecond laser pulses focused inside transparent silica [29, 30]. The utilized glass allows us to use light of wavelengths shorter than those used in AlGaAs waveguides in previous demonstrations of Anderson localization of light in arrays with diagonal disorder. Glass waveguides also mitigate the low coupling efficiency of light into high-refractive-index ($n_{\text{AlGaAs}} \approx 3.3$) waveguides. In our arrays, the waveguides are all identical, i.e. they all have the same propagation constant, while the coupling coefficients are randomized by changing the relative positions of the waveguides. We observe that extended states in a periodic waveguide array become exponentially localized states when the localization length is shorted [31] by increasing the amount of waveguide positional disorder. The excellent agreement between experimental observations and theoretical calculations is a testament to the accuracy of the waveguide fabrication technique.

Random Walk in Waveguide Arrays

The propagation of an optical field along a lossless waveguide array with nearest-neighbor evanescent coupling can be described, in general, by the equation

$$i\frac{dE_n}{dz} + \beta_n E_n + \mathscr{C}_{n,n+1}E_{n+1} + \mathscr{C}_{n,n-1}E_{n-1} = 0 \tag{2.1}$$

where E_n is the electric field amplitude at the nth waveguide (n = 1,2,$\cdots$,N), β_n is the propagation constant of the n^{th} waveguide, and $\mathscr{C}_{n,n\pm1}$ is the coupling coefficient between adjacent waveguide elements. We assume lossless propagation and set $\mathscr{C}_{n,n\pm1} = \mathscr{C}_{n\pm1,n}$. The magnitude of the coupling coefficients depends exponentially on the separation between adjacent waveguides [30].

We begin by considering a periodic array ($\mathscr{C}_{n,n\pm1} = \mathscr{C}_0$) of identical $\beta_n = \beta_0$ waveguides, where-

upon Eq. (2.1) simplifies to

$$i\frac{dE_n}{dz} + \mathscr{C}_0 \left(E_{n+1} + E_{n-1}\right) = 0 \tag{2.2}$$

For a single-input-site excitation $E_{n_0} = A_0\delta_{n,n_0}$ at $z = 0$, the field in the nth waveguide is given by

$$E_{n,n_0}(z) = A_0 i^{n-n_0} J_{n-n_0}\left(2\mathscr{C}_0 z\right) \tag{2.3}$$

where $J_n(x)$ represents a Bessel function of order n, and the output intensity distribuation is

$$I_{n,n_0}(z) \propto |J_{n-n_0}\left(2\mathscr{C} z\right)|^2. \tag{2.4}$$

This output distribution exhibits two off-center lobes where most of the optical energy is concentrated, and whose distance from the transverse location of the excitation site increases linearly with the propagation length along the array (see Fig. 2.1a). This is characteristic of discrete diffraction [18], which is in stark contrast to free-space diffraction where most of the light is concentrated in a central lobe.

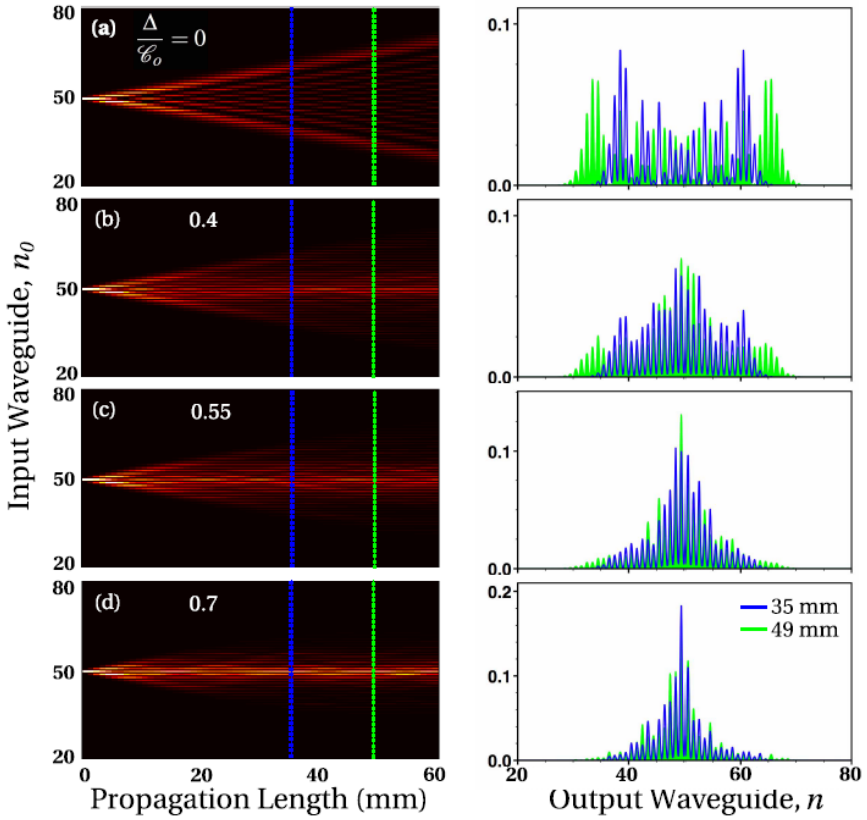

Figure 2.1: Numerical simulation of optical field propagation when light is injected into the 51st waveguide in a 101-waveguide array. The arrays used in (a) to (d) have increasing degree of disorder. Each plot results from averagin the intensities of 41 realizations of random disordered arrays described by a uniform propability distribution function having a mean value $\mathscr{C}_0$ =1.8cm^{-1} and width 2Δ, for disorder parameters $\Delta/\mathscr{C}_0 = 0, 0.4, 0.55$ and 0.70 respectively. The average output intensity distributions for propagation lengths 35 mm (blue) and 49 mm (green), respectively, corresponding to the lengths of the two samples used, are shown on the right.

Disorder can be introduced into a waveguide array by one of two strategies. In the first, one randomly changes the waveguide width, while keeping the distance between waveguide centers constant. As a result, the propagation constants β_n vary from one waveguide to another in the range$\beta_0 \pm \Delta$, while the coupling coefficients are approximately constant, $\mathscr{C}_{n,n\pm1} = \mathscr{C}_0$ [11, 12]. This disordered array corresponds to the diagonal-disorder model in Andersons original formula-

tion. In the second strategy, the waveguides are all identical, but the separation between adjacent waveguides is randomized. The propagation constant is the same for all the waveguides $\beta_n = \beta_0$, while the coupling coefficients become random in the range $\mathscr{C}_0 \pm \Delta$. Such an array corresponds to the *off-diagonal-disorder* model. In this paper, we focus on waveguide arrays involving off-diagonal disorder. Propagation in such an array is described by the following equation,

$$i\frac{dE_n}{dz} + \mathscr{C}_{n,n+1}E_{n+1} + \mathscr{C}_{n,n-1}E_{n-1} = 0 \tag{2.5}$$

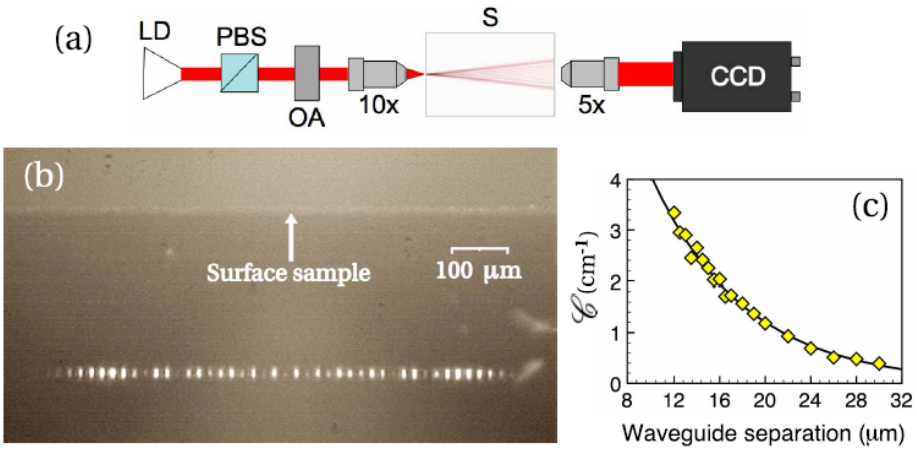

Figure 2.2: (a) Experimental setup. LD: laser diode (780 nm); PBS: polarizing beam splitter; OA: optical attenuator; 5× (NA=0.1) and 10× (NA=0.25) microscope objectives; S: Waveguide Array sample. (b) CCD image of the periodic waveguide array output (period = 17 μm, and distance from the top of fused silica slab $\approx$ 250 μm) when a single waveguide is excited at the input. (c) Measured dependence of the coupling coefficient $\mathscr{C}$ on the waveguide separation for directional couplers fabricated with the same parameters as the arrays.

In Figs. 2.1b-d we present numerical simulations of the intensity of a field propagating along such an array averaged over 41 realizations of the random disordered parameters $\mathscr{C}_{n,n\pm1}$, chosen according to a uniform probability distribution with a mean value $\mathscr{C}_0$ and width 2Δ, for disorder

parameters $\Delta/\mathscr{C}_0 = 0$, 0.4, 0.55, and 0.70. Note the transition from extended (Fig. 2.1a) to exponentially localized (Fig. 2.1d) optical states with increasing disorder.

The Waveguide Array

The waveguides used in this study were fabricated using 800-nm-wavelength femtosecondlaser pulses focused at a depth of $\approx$ 250 microns below the surface of polished bulk fused-silica glass [29, 30], inducing permanent refractive index changes.

A computer-controlled positioning system allows one to write waveguides [29] of transverse size 4×12 μm. At a wavelength of 800 nm, these are single-mode waveguides with NA = 0.06 [30]. We prepared two identical samples each consisting of four waveguide arrays, but having different lengths, 35 mm and 49 mm, referred to hereon as short and long samples, respectively. The waveguides in all of the arrays in both samples are identical. Each array consists of 101 waveguides with nearest-neighbor evanescent coupling. The first array in each sample is periodic with inter-waveguide separation of 17 μm (numerical simulation of optical field propagation when light is injected into a single waveguide of the periodic array is shown in Fig. 2.1a), corresponding to a coupling coefficient $\mathscr{C}_0 = 1.8$ cm^{-1} (Fig. 2.2c). The other arrays are disordered with random (off-diagonal) coupling coefficients. The values of the coupling coefficients in each array are described by uniform probability distribution functions all having the same mean value $\mathscr{C}_0$, but with increasingly larger width 2Δ (Fig. 2.1b-d). According to the exponential dependence of $\mathscr{C}_0$ on the waveguide separation (Fig. 2.2c), such a uniform distribution of coupling coefficients can be generated by imposing an exponential distribution on the separation [30].

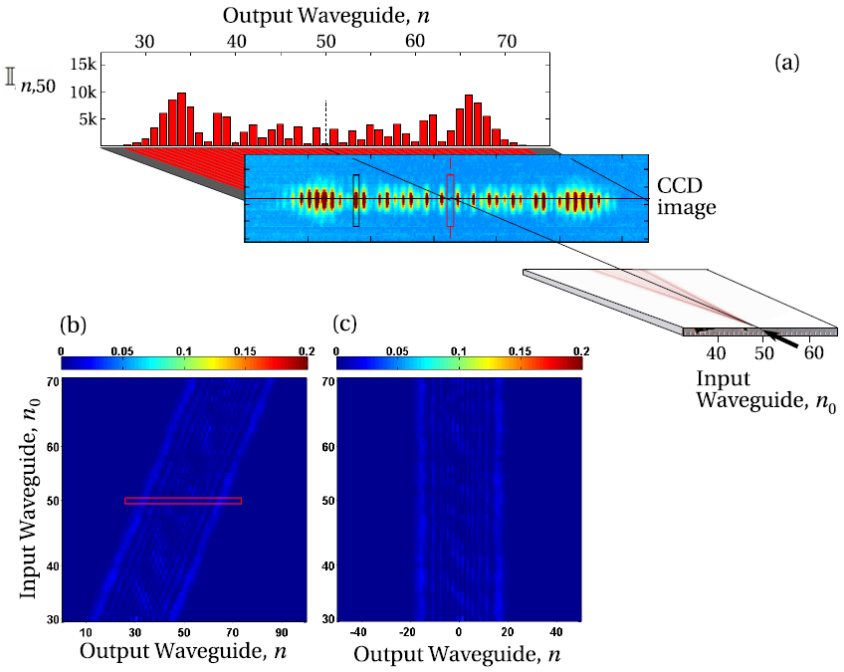

Figure 2.3: Data acquisition and analysis. Panel (a) presents data for light injected into the 50th waveguide (n_0 = 50) of the long periodic array. The intensity at the output of the waveguide array is captured with a CCD camera (shown in the middle). The image is then post-processed to extract the discrete intensity distribution ($\mathbb{I}_{n,50}$) by integrating over rectangular areas 10×30 pixel each centered on the center of each waveguide (n) shown as the black rectangle. The central red rectangle on the CCD image in panel (a) indicates the location of the excitation site. The discrete intensity distribution, $\mathbb{I}_{n,50}$ is shown as the red bar-plot. The brightness image in panel (b) displays the distribution, $\mathbb{I}_{n,n_0}$ of the intensity of the light measured at the output of the waveguides (n) when only waveguide n_0 is illuminated. The red rectangle on panel (b) indicates the output distribution for light injected into the 50th waveguide. In panel (c) the displaced distribution, $\mathbb{I}_{n+n_0,n_0}$ is shown. Each distribution of the measured intensity is displaced such that it is centered about the illuminated waveguide. Only the middle 41 waveguides are illuminated (one at a time) with the ordinate marking the illuminated waveguide.

Optical Measurement System

The experimental setup used to observe the transition to Anderson localization in the above described optical waveguide arrays is shown in Fig. 2.2. A horizontally polarized beam from a diode laser at 780 nm is attenuated and focused by a 10× microscope objective (NA=0.25) into a single

waveguide in the array (see Fig. 2.2a). The waveguide array output is imaged on a CCD camera using a 5× microscope objective (NA= 0.1). A typical output intensity distribution for single-site excitation in the periodic array in the long sample is shown in Fig. 2.2b, demonstrating clearly the expected discrete diffraction pattern.

The data recording and analysis procedure is sketched in Fig. 2.3. A single waveguide is illuminated and the intensity of the light at the output of the waveguide array is captured by the CCD camera. The realization shown in Fig. 2.3a was obtained by injecting light into the 50th waveguide in the long-sample periodic array. The 2D image was post-processed to extract a discretized 1D intensity distribution. A rectangle of size 10×30 pixels that covers the image of a waveguide was integrated and a background term was subtracted. The resulting discrete intensity distribution $\mathbb{I}_{n,50}$ is shown as the red-bar plot.

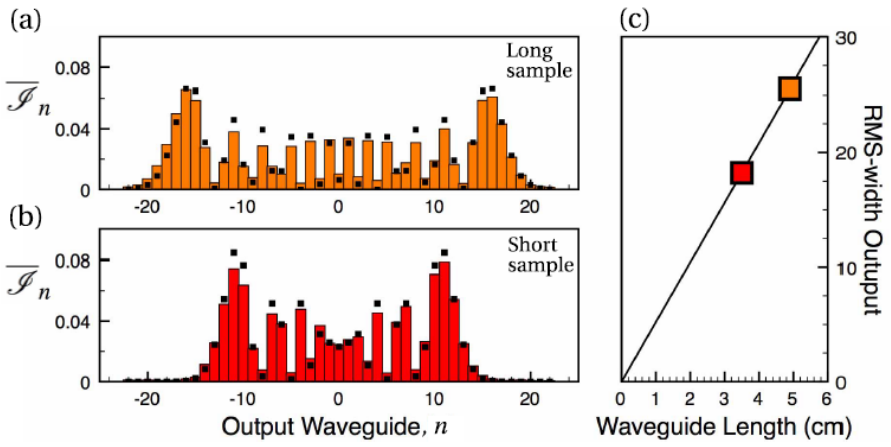

Figure 2.4: Average displaced distribution $\bar{\mathscr{I}}_n$ for long (a) and short (b) periodic waveguide arrays. The black squares represent a theoretical best-fit with $\mathscr{C}_0 \approx 1.79\text{cm}^{-1}and1.80\text{cm}^{-1}$ for the short and long arrays, respectively. The root-mean-square (RMS) width of the experimental distributions (≈ 18.0 and ≈ 25.4) are shown in (c) as function of the array length. The line represents the best-fit to the linear ballistic expansion as a function of the array length with $\mathscr{C}_0 \approx 1.81\text{cm}^{-1}$.

The uniformity of the waveguide losses is attested by the fact that the total output power $\mathbb{P}_{n_o} =$

$\sum_n \mathbb{I}_{n,n_o} = \mathbb{P}$ is constant $\forall n_o$ (for fixed input power). We normalized the output intensity with respect to $\mathbb{P}$, $\mathscr{I}_{n,n_o} = \mathbb{I}_{n,n_o}/\mathbb{P}$ and then averaged the output distributions for different excitation sites after shifting them by the index of that excitation site (see Fig. 2.3c),

$$\bar{\mathscr{I}}_n = \sum_{n_o} \mathscr{I}_{n+n_0,n_0}. \tag{2.6}$$

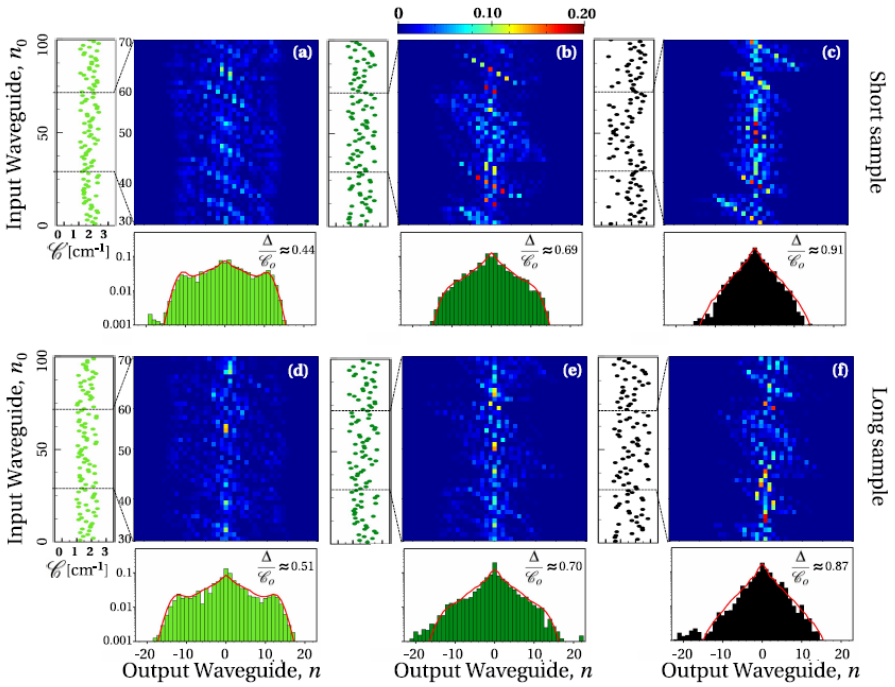

Figure 2.5: Effect of disorder on the propagation of light through 101-waveguide arrays in the short (first row, a-c) and long (second row, d-f) samples. The two rows correspond to disorder parameters $\Delta/\mathscr{C}_0 \approx$ 0.44, 0.69 and 0.91 for the short sample, and 0.51,0.70 and 0.87 for the long sample. The color plot in each panel shows the displaced distributions $\mathscr{I}_{n+n_0,n_0}$ at the output. Each row in the plot corresponds to the output intensity distribution for a single point excitation at n_0 after shifting it by n_0. Only the middle 41 waveguides are illuminated (one at a time) with the ordinate marking the illuminated waveguide. The average of the displaced distributions, $\bar{\mathscr{I}}_n$, for all 41 waveguides is plotted at the bottom of each panel with the red line showing the result of a numerical simulation with $\mathscr{C}_0$ and Δ as fitting parameters.

The resulting averages are shown in Fig. 2.4 for the short and long periodic arrays. This procedure is justified since the characteristics of the array are shift invariant. This necessitates excluding edge effects which occur if the ends of the array are excited, as investigated by Szameit *et al*. [26]. Therefore, we excite the input waveguides n_o = 31...71, which guarantee that the output intensity distribution does not extend to the edges of the arrays. A best-fit for these distributions to the theoretical expectation $|J_n(2\mathscr{C}_0 z)|^2$ allows us to evaluate the coupling coefficient to be $\mathscr{C}_0 \approx 1.79$ cm$^{-1)}$ and 1.80 cm$^{-1)}$ for the short and long arrays, respectively, defined by numerical simulation fittings. Further confirmation of our results comes from verifying that the separation of the lobes in the ballistic expansion increases linearly with sample length. We have evaluated the root-mean-square (RMS) width of the experimental distributions $math\bar{s}crI_n$, and fitted them with the coupling coefficient $\mathscr{C}_0$ as the only free parameter, as shown in Fig. 2.4.

Anderson Localization in Waveguide Arrays with Off-Diagonal Disorder

We next proceed to examine wave propagation through waveguide arrays with off-diagonal disorder. The coupling coefficients between adjacent waveguides in a single array were chosen such that they belong to a uniform probability distribution function having mean value $\mathscr{C}_0$. The width of the distribution 2Δ increases from one array to the next, corresponding to increasing disorder. The values of $\mathscr{C}_0$ and Δ have been determined by fitting the experimental data with numerical simulations: $\mathscr{C}_0$ ($\approx$ 1.79 cm^{-1} and 1.50 cm^{-1} for the short and long arrays, respectively) defines the distance between the lobes of the ballistic expansion, which is still visible in Fig. 2.5a and 2.5d, while Δ defines the central exponential peak. The disorder parameters for our arrays are found to be $\Delta \approx 0.44$, 0.69 and 0.91 for the short sample, and 0.51, 0.70 and 0.87 for the long sample. The experimental setup and data analysis procedure used with the disordered arrays were identical to those described above for the periodic arrays (see Fig. 2) after accounting for the random locations of the waveguides in these off-diagonal disordered arrays. We have also used here the same post-

processing data analysis to obtain the displaced distributions $\mathscr{I}_{n+n_o,n_o}$ and the average displaced distribution $\bar{\mathscr{I}}_n$ for each array.

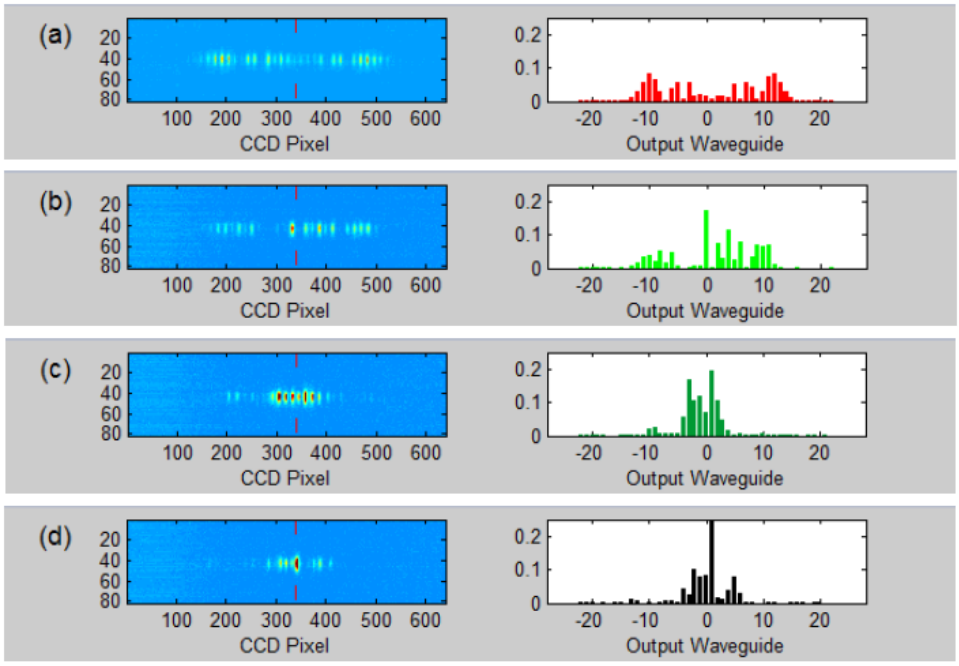

Figure 2.6: Single-frame excerpts from video recordings. On the left we display the recorded intensity distribution at the output of the short waveguide array when the middle 41 input waveguides are illuminated one at a time, while on the right the cumulative averaged discrete intensity distribution is updated. (a) Periodic array ; (b) array with disorder parameter $\Delta/\mathscr{C}_0 \approx 0.44$; (c) array with $\Delta/\mathscr{C}_0 \approx 0.69$; (c) array with $\Delta/\mathscr{C}_0 \approx 0.91$.

As we repeat the experiment in arrays with progressively larger off-diagonal coupling disorder, shortening the localization length with respect to the ballistic spreading, we observe at the array outputs a clear enhancement of the exponentially localized (Anderson-localized) optical states for both samples [31]. As shown in Fig. 5, we observe that the ballistic expansion in the periodic array evolves, with increasing disorder, into an intermediate regime at $\Delta/C_0 \sim 0.5$ that exhibits characteristics of both extended and localized states (Fig. 5a,d). Finally Anderson localization is clearly evident at $\Delta/C_0 \sim 0.9$ (Fig. 5c,f).

It is worth noting that as we scan the beam injected into individual waveguides across a disordered array, besides the shift due to the scanned input, the output intensity distribution changes. This results from the fact that the spreading optical field encounters a random coupling environment as we move across the array. In contrast, the individual realizations at the output of the periodic array are almost all identical (modulo the shift). Anderson localization is then established for the disordered array by averaging the different realizations resulting from spatial scanning the input beam. These features are brought together in the movies in Fig. 2.6. On the left we depict the individual output intensity distributions resulting from scanning the excited waveguides at the input, and in the right we display an updated cumulative average. In the case of the periodic array, averaging has little effect.

The localized states observed by averaging over multiple realizations of the gradually increased disorder is demonstrated in Fig. 2.7. The RMS-widths of the output intensity distribution measured for the two arrays with different length are compared to numerical simulations for two methods of statistical averaging over the waveguide disorder. We note that our results demonstrate that ensemble statistical averaging, achieved by coupling into a single waveguide in a set of independent disordered arrays (sampling average) is equivalent to spatial scanning through multiple waveguides in the same off-diagonally disordered array (shifted average). Finally to highlight the exponential decay of the Anderson-localized state away from its center, we plot in log-scale the average displaced distribution In for short and long samples in the inset of Fig. 2.7. The exponential decay fits until we reach the noise level of the data.

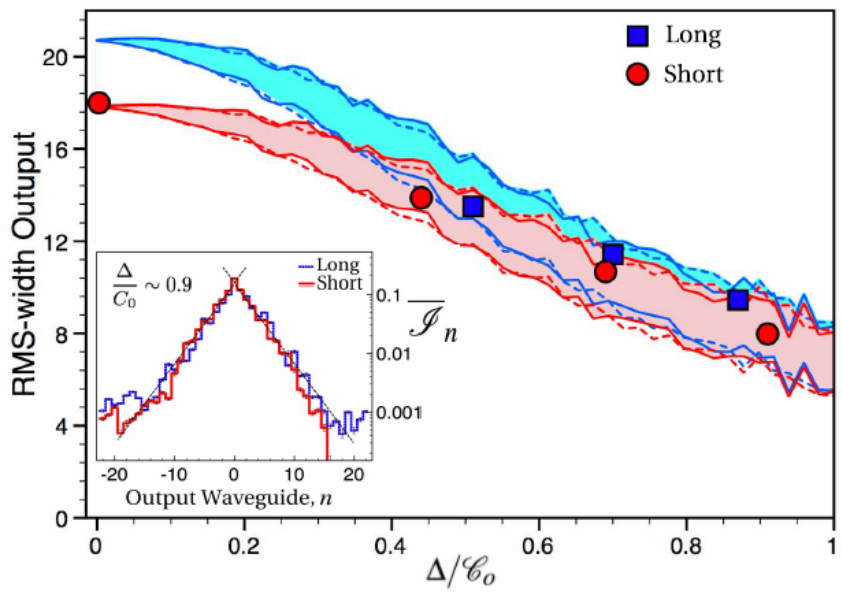

Figure 2.7: RMS width as function of the disorder parameter $\Delta/\mathscr{C}_0$ for the short (red-circle symbols) and long array (blue-square symbols). The colored bands represent the range of values of the RMS-width a standard deviation around the mean value. For each value of the disorder parameter, RMS-width and its standard deviation have been evaluated by averaging over 21×40 disorder realizations for the sampling average approach (dashed lines), while 21 disorder realizations and 40 shifted input waveguides have been considered for the shifting average approach (solid lines). Inset: average displaced distribution, $\overline{\mathscr{I}}_n$ for short and long arrays with disorder parameter $\Delta/\mathscr{C}_0 \approx 0.9$. The log-scale plot highlights the exponential decay of the Anderson-localized states. The dotted-lines are a guide for the eye.

Conclusion

We have observed the gradual passage from extended to Anderson-localized states in near infrared light propagation through waveguide arrays of different lengths having a uniformly distributed off-diagonal coupling disorder. Precise fabrication techniques have allowed us to control the disorder parameter and enabled us to obtain experimental measurements confirming theoretical predictions with good accuracy, including the exponential behavior of the Anderson localized state.We have supported the experimental results with numerical simulations for both shifting and sampling

statistical averaging methods and shown that both methods yield equivalent results of the same precision.

Acknowledgements

This work was supported by CREOL, The College of Optics and Photonics, at the University of Central Florida, and Deutsche Forschungsgemeinschaft (Research Unit 532 and Leibniz program).

CHAPTER 3: ENTANGLED PHOTON PAIRS IN PHOTONIC LATTICES: PART I

Introductory Remarks on Experiment Two

The following paper was originally published in Physical Review Letters [14]. It details research I performed coupling spatially correlated, entangled photon pairs into periodic and disordered photonic lattices and measuring the second order correlation function $G^{(2)}(x_1, x_2)$ at the output of the array. In this report, I first show simulation and measurement of Anderson localization on the single photon level. As discussed, this result does not address new physics beyond that of classical light and again requires shifting and averaging to obtain the localization signature. However, the results become markedly different once I proceed onto spatially extended, entangled two photon states. The input optical system, which lies between the nonlinear crystal generating the entangled photon pair and the input face of the waveguide array, is an imaging system, meaning the two photons which are generated at the same point in the nonlinear crystal are imaged to the same waveguide. The correlated photon pair then traverses the array. In the periodic array, the two dimensional ballistic distribution is seen oriented along the $x_1 = x_2$ axis. We note that the ballistic distribution corresponding to classical propagation beginning in a single waveguide can be recovered observing the diagonal marginal, obtained by summing along the $G^{(2)}(x_1, x_2)$ along the $x_1 = x_2$ axis. The resulting marginal ballistic distribution corresponds to propagation of classical light in an array of twice the length. In the weakly and strongly disordered arrays, I observed a new phenomenon termed Anderson co-localization, in which the two photons localize in correlation space along the $x_1 = x_2$ axis. The exponential signature of Anderson localization is observed when examining the positive marginal distribution, which is again obtained by summing the $G^{(2)}(x_1, x_2)$ along the $x_1 = x_2$ axis. Obtaining this does not require the shift and averaging

procedure that is required in the classical case. In this way, we reveal that the entangled two photon state has its correlations largely preserved after propagation in the disordered array, which may be unexpected, as strong environmental disorder is usually considered to be detrimental to any expression of entanglement.

Einstein-Podolsky-Rosen Spatial Entanglement in Ordered and Anderson Photonic Lattices

G. Di Giuseppe, L. Martin, A. Perez-Leija, R. Keil, F. Dreisow, S. Nolte, A. Szameit, A.F. Abouraddy, D.N. Christodoulides and B.E.A. Saleh, Physical Review Letters, 110, 150503, 2013.

Introduction

Quantum information processing promises exponential speedup of intractable computational problems, secure cryptographic key distribution, and exotic communications protocols such as teleportation [6]. Manipulating entangled multipartite quantum states on a chip is now paving the way towards scalable platforms for quantum information processing and quantum communications [32, 33, 34, 35]. Among the potential physical platforms, photonic realizations offer benefits in terms of simplicity of generating and transforming entangled quantum states [36]. Advances in micro- and nanofabrication have recently enabled a new generation of on-chip quantum photonic devices that may enable largescale linear quantum computation [37] and the observation of fundamental processes such as quantum walks [38, 22]. To fully exploit the information-carrying capacity of any physical system, all relevant degrees of freedom, whether spin, frequency, or spatial, must be utilized. Thus far, photon polarization [39] or two-path realizations [35] have been the preferred on-chip qubit embodiment. The quest for increasing the information-carrying capacity

of a single photon necessitates the use of other degrees of freedom that offer higher dimensionality. It is thus important to explore new classes of integrated photonic configurations capable of harnessing such high-dimensional degrees of freedom. Clearly, the benefits accrued will be even greater if entanglement is utilized in such large-dimensional systems. In particular, spatially entangled photon pairs [40] whose counterintuitive properties were the starting point of the Einstein-Podolsky-Rosen (EPR) gedankenexperiment [1]naturally inhabit a high-dimensional Hilbert space [41, 42]. To date, realizations of integrated photonic quantum circuits first project the spatial degree of freedom onto a single mode, thereby stripping the spatial entanglement, in order to couple into on-chip waveguide systems [35, 39, 43]. Quite recently, the study of the evolution of two-photon states in one-dimensional waveguide lattices was suggested by Bromberg et al. [44]. Here we experimentally demonstrate large-scale quantum walks using two-photon spatially extended EPR states launched into on-chip multiport lattice circuits with and without disorder. In one configuration, quantum walks through a periodic waveguide array convert spatially correlated EPR pairs into anticorrelated pairsa spatially extended inverse of Hong-Ou-Mandel interference [45]. In a different configuration, a lattice with controllable disorder halts the spreading of each photon of a pair in a separable stateleading to the first demonstration of Anderson localization (AL) [13] at the single-photon level. When entangled EPR photons are launched into this array, we observe a new disordermediated two-photon interference effect. The extended EPR photons do not localize. In this case, their spatial correlations unexpectedly survive the disordered quantum random walk, resulting in localization in fourth-order correlation space, or colocalization [46, 47]. In our experiment (Fig. 1-i) we produce EPR photon pairs by optical spontaneous parametric down-conversion from a nonlinear crystal (NLC)[40]. These entangled photon pairs are then imaged to the input plane of an integrated multiport photonic lattice. Entangled quantum walk experiments were carried out in three different lattices, each consisting of a large array of 101 evanescently coupled, parallel, identical, single-mode, low-loss optical waveguides inscribed in silica glass [30]. In this setting, the waveguides have identical propagation constants, and the inter-waveguide coupling is

determined by their separation (Fig. 3.1-ii and Fig. 3.1-iii).

The evolution along z of the quantized-field operators $a_n^\dagger$ in the nth waveguide in this tight-binding lattice is determined by the Heisenberg equation of motion in the interaction picture [44], $-i\frac{da_n^\dagger}{dz} = \kappa_{n,n-1}a_{n-1}^\dagger + \kappa_{n,n+1}a_{n+1}^\dagger$ where $\kappa_{n,n-1}$ is the coupling coefficient between adjacent sites. Integration of this equation yields $\boldsymbol{A}^\dagger(z) = \hat{\boldsymbol{U}}(z)\hat{\boldsymbol{A}}^\dagger(0)$ where $\hat{\boldsymbol{A}}^\dagger(z) = \left[a_n^\dagger(z)\right]_{n=1}^N$, $\hat{\boldsymbol{U}}(z) = \exp^{i\hat{\boldsymbol{H}}z}$, and $\hat{\boldsymbol{H}}$ represents the coupling-coefficient matrix. In experiments using two-photon states, this transformation applies to the quantized field operators of each photon.

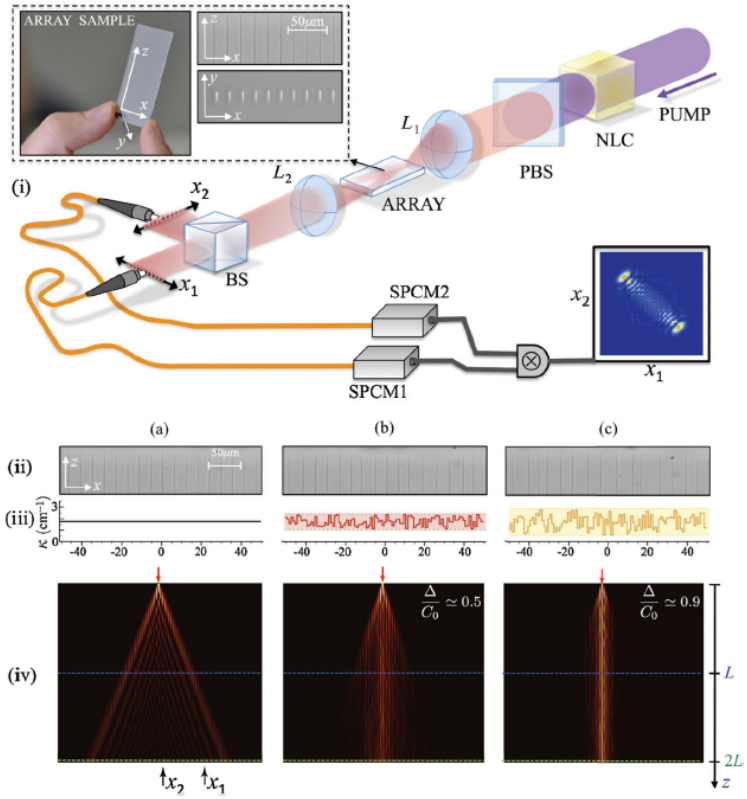

Figure 3.1: (i) Experimental setup. A pump laser incident on a NLC generates spatially entangled photon pairs that are coupled into a waveguide array using a lens L1 (an achromatic doublet, focal length 30 mm) in an imaging configuration. The distance from the nonlinear crystal to L1 and the distance from L1 to the waveguide array were chosen to demagnify the spatial extent of the photon pairs by a factor of 4. A lens L2 (an achromatic doublet, focal length 40 mm) images the photon pairs emerging from the array with a magnification factor of 6.5 to two identical planes x_1 and x_2 separated using a beam splitter (BS), and are collected by two scanning fibers coupled to detectors SPCM1 and SPCM2. A coincidence circuit provides the correlation function $G^{(2)}(x_1, x_2)$. The pump beam is removed after the NLC using a polarizing beam splitter (PBS). Inset: Photograph of the waveguide array sample (left), a phase-contrast microscope image of a section of the periodic array taken from the top of the array showing the waveguides along z (top right), and an optical micrograph of white light emerging from the periodic array output (bottom right). (ii) Phase-contrast microscope images of a section of each waveguide array. (iii) Values of the nearest-neighbor coupling coefficients for each array. (iv) Calculated evolution of a one-photon state along each waveguide array when a single waveguide is excited. Distances L = 5 cm (the physical length of the arrays) and $2L$ are highlighted. Columns: (a) periodic, (b) weakly disordered, and (c) highly disordered arrays.

In our work we consider three such arrays of length $L = 5$ cm: a periodic array $\kappa_{n,n-1} = \kappa_o, \forall n$

(Fig. 3.1-ii-a); a weakly disordered array with coupling constants chosen from a uniform random distribution $\kappa \in [\kappa_o - \Delta, \kappa_o + \Delta]$ with mean κ_o and normalized width $\Delta/\kappa_o = 0.5$ (Fig. 3.1-ii-b); and a strongly disordered array with $\Delta/\kappa_o = 0.9$ (Fig. 3.1-ii-c). The array output plane is imaged to two identical planes, x_1 and x_2 (Fig. 3.1-i). Two fibers connected to single-photon-sensitive detectors are scanned in these planes to collect the emerging photons at the imaged waveguide locations in order to register the coincidence rate $G^{(2)}(x_1, x_2)$ [48]. The dynamics of onephoton states when launched into a single waveguide are depicted in Fig. 3.1-iv for these three cases. The entangled photon pairs produced in our experiment are in a quantum-correlated two-photon state as previously demonstrated [40, 49]. Each pair is always injected together into a waveguide. This waveguide can be any of the $N = 101$ sites covered by the spatial extent M of the state. The two-photon EPR state, or multipath entangled state, covering M discrete lattice points takes the form

$$|\Psi_{\rm EPR}\rangle = \frac{1}{\sqrt{M}}\{|2_1, 0_2, \cdots, 0_M\rangle + |0_1, 2_2, \cdots, 0_M\rangle + \cdots + |0_1, 0_2, \cdots, 2_M\rangle\} \tag{3.1}$$

where the indices refer to the sites. The quantum correlations in this spatially extended state $|\Psi_{\rm EPR}\rangle$ are such that the two photons are always on the same lattice site, but with equal probability $\frac{1}{M}$ of being at any of the M excited sites. In our experiments, $M = 20$ and the uniform probability distribution is approximated by a truncated broad Gaussian distribution. In contrast, a separable two-photon state is excited if they are both launched into a single waveguide k

$$|\Psi_{\rm sep}\rangle = |0_1, 0_2, \cdots, 0_{k-1}, 2_k, 0_{k+1}, \cdots, 0_M\rangle\,. \tag{3.2}$$

In this separable state, the two photons are independent. We stress that current experimental approaches that make use of integrated devices have so far relied on first coupling the photon pairs

into a single-mode fiber, which destroys their spatial correlations. Here we obviate this limitation through free-space imaging of the EPR state from the NLC to the chip, thereby loading spatial entanglement into the photonic circuit. This scheme allows the high dimensionality of the EPR state in Eq. (3.1) to be exploited in an integrated quantum photonic arrangement to observe entangled quantum walks.

The propagation dynamics of a two-photon state along the three arrays depends on the initial state. If $|\Psi_{\rm sep}\rangle$ is injected into a single waveguide in any of the arrays, the output coincidence rate separates into a product $G^{(2)}(x_1, x_2) = G^{(1)}(x_1, x_1)G^{(1)}(x_2, x_2)$ of single-photon distributions $G^{(1)}(x_1, x_1)$ and $G^{(1)}(x_2, x_2)$ [11,24]. When light in the state $|\Psi_{\rm EPR}\rangle$ is coupled into the array, $G^{(2)}(x_1, x_2)$ no longer factorizes and the dynamics are altogether different.

Experiment

The experimental setup is illustrated in Fig. 1. Photon pairs are produced via collinear degenerate type-I optical spontaneous parametric down conversion from a $LiIO_3$, 1.5-mm thick nonlinear crystal excited with a pump laser (CW Coherent Cube laser diode, 80-mW power, 404-nm wavelength, vertically polarized). The photon pairs (horizontally polarized, centered at 808 nm) are coupled into the waveguide array using an achromatic doublet lens of 30-mm focal length in a telescopic imaging arrangement. The pump beam is removed after the NLC using a Glan-Thompson polarizing beam splitter and a red long-pass filter after the array. This arrangement is similar to that previously used in Ref. [49] where we demonstrated a violation of Bells inequality, thereby ensuring the high degree of entanglement of the state produced here. The photon pairs emerging from the array are imaged using an achromatic doublet lens of 40-mm focal length to two identical planes x_1 and x_2 separated using a nonpolarizing BS and are collected by two fibers (multimode, 62.5-μm core diameter) coupled to single-photon-sensitive detectors SPCM1 and SPCM2 (Perkin-Elmer,

SPCM-AQR-15-FC). A coincidence circuit measures the correlation function $G^{(2)}(x_1, x_2)$ using a 3-ns window. The waveguide elements, which are inscribed in silica glass, are all identical and single mode (width 4 μm, height 11 μm, NA 0.045, length 5 cm). In the periodic array, the center-to-center waveguide separation is 17μm and the measured coupling coefficient $\kappa_0 \approx 1.7\text{cm}^{-1}$. The disordered arrays are implemented by varying the distance between adjacent guides such that a uniform distribution of the coupling κ is obtained [46, 9]. In analyzing the data from these finite arrays, we have carried out simulations using the actual distribution of coupling coefficients. A more complete statistical analysis was carried out in Refs. [47, 9].

Periodic array

We first investigate the evolution of $|\Psi_{\text{EPR}}\rangle$ and $|\Psi_{\text{sep}}\rangle$ along the periodic array (Fig. 3.2): (i) When the $|\Psi_{\text{sep}}\rangle$ state is excited, the measured coincidence rate $G^{(2)}(x_1, x_2)$ features four symmetric peaks (Fig. 3.2-iii-a) and is separable into the product of two pairs of ballistic peaks for each photon (Fig. 3.1-iv-a). These peaks signify that if a photon is detected on one side of the array, then its twin is equally likely to be detected on the same side (the diagonal peaks) or at its mirror symmetric location with respect to the input site (the off-diagonal peaks). As in the case of a beam splitter with a two-photon state at one input port, the two photons are equally likely to emerge from the same or different ports. Here the array plays the role of a spatially extended beam-splitting photonic circuit.

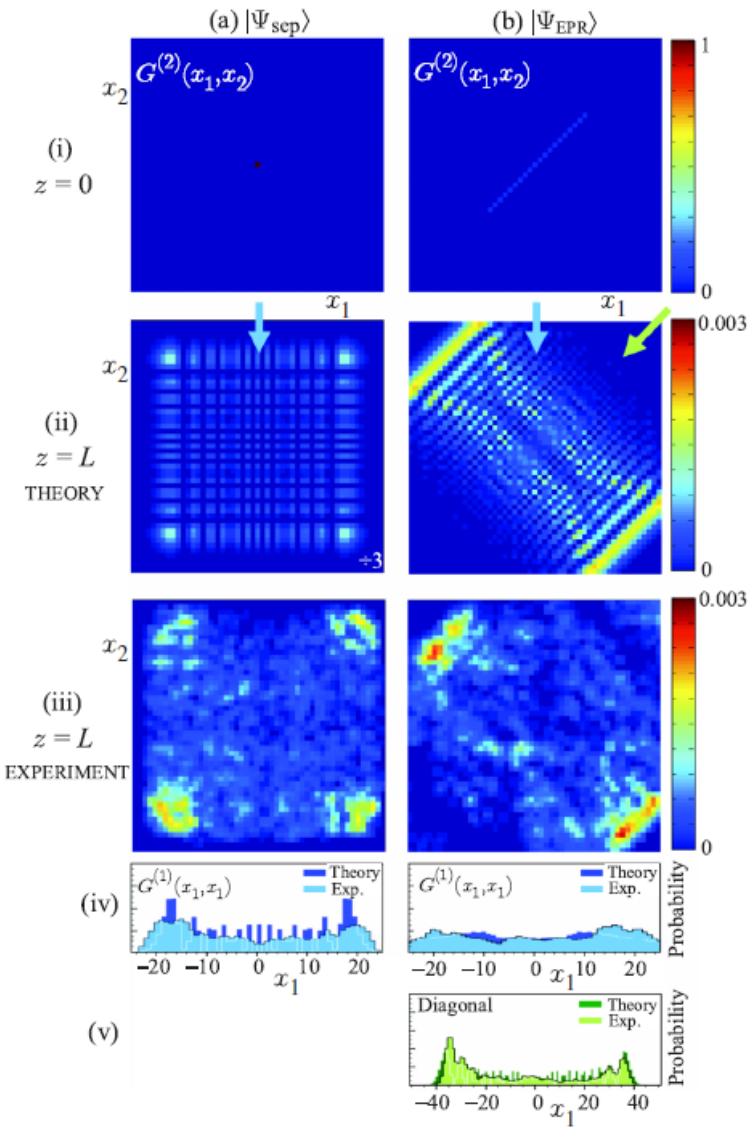

Figure 3.2: Observation of the correlation function $G^{(2)}(x_1, x_2)$ in a periodic lattice. Column (a) corresponds to the separable state $|\Psi_{\rm sep}\rangle$ and column (b) to the entangled state $|\Psi_{\rm EPR}\rangle$. (i) Expected $G^{(2)}(x_1, x_2)$ at the input. (ii) Theoretical and (iii) measured coincidence rate at the output. (iv) Calculated and measured singles distribution $G^{(1)}(x_1, x_1)$ at the output. (v) Calculated and measured diagonals distribution at the output for$|\Psi_{\rm EPR}\rangle$. The width of the horizontal axis for x_1 in (v) is twice that in the rest of the figure.

Consequently, the singles distributions are identical to the single-photon (or classical) outcome

$G^{(1)}(x_1, x_1)$ for the same array (Fig. 3.2-iv-a). This arrangement corresponds to a two-photon continuous quantum random walk [50, 51], where each photon in the pair evolves independently. (ii) The two-photon dynamics are dramatically altered when $|\Psi_{\rm EPR}\rangle$ is excited instead. The two diagonal peaks that appear in the separable case are here suppressed (Fig. 3.2-ii-b and Fig. 3.2-iii-b), leaving only two prominent off-diagonal peaks, as predicted theoretically in Ref. [47]. Surprisingly, even though the two photons at the input are always in the same lattice site, at the end of the quantum walk they emerge from opposite sides of the array with respect to the center. Furthermore, $G^{(2)}(x_1, x_2)$ is not factorizable and the singles correspond to the evolution of a spatially extended mixed one-photon state (Fig. 3.2-iv-b). Nevertheless, examining the diagonal marginal distribution (diagonals), resulting from integrating $G^{(2)}$ along $x_1 = x_2$ [19], brings forth an unexpected result (Fig. 3.2-v-b). In general, the diagonals reveal the distribution of separations between the two photons emerging from the array. Here the diagonals distribution equals that resulting from the evolution of a one-photon state that is coupled into a single lattice site and after propagating for a distance $2L$twice the length of the physical array [47]. The two off-diagonal peaks, along the $x_1 = -x_2$ axis, in the periodic array signify that the two photons always emerge on opposite sides of the array, although the pairs are coupled into the same waveguides at the input. In essence, this observation corresponds to the reverse of the usual two-photon Hong- Ou-Mandel interference effect [45] where two photons enter different ports of a beam splitter and emerge together from one of the output ports. Our arrangement realizes the inverse of this effect in a spatially extended configuration across the waveguide array.

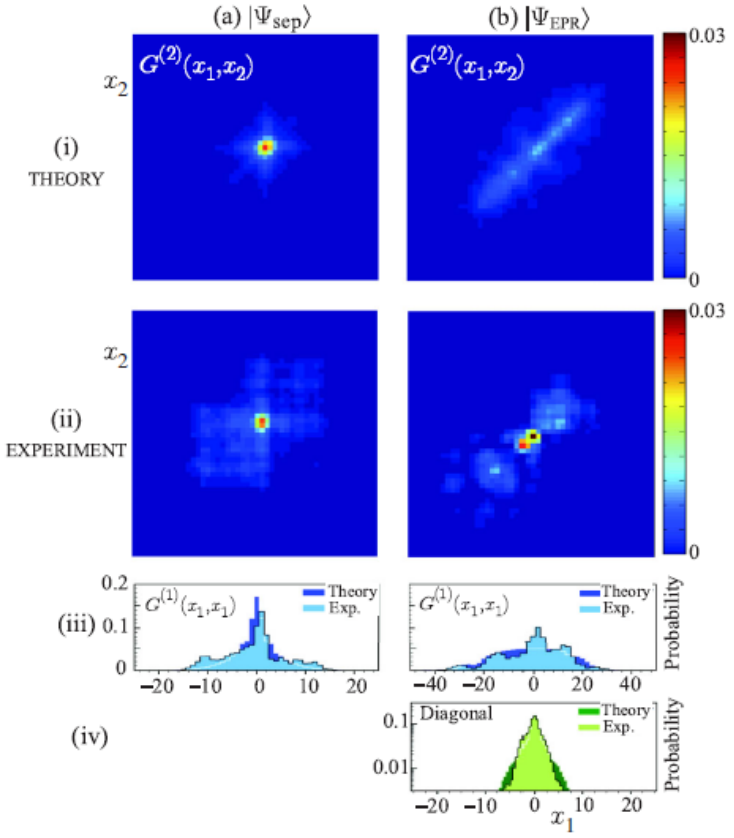

Figure 3.3: Same as in Fig. 3.2 for the disordered Anderson lattice ($\Delta/\kappa_0 = 0.9$).

Disordered array

We now investigate how the two photon quantum walk is affected in the extreme limit of a strongly disordered lattice that is expected to halt the spreading of single-photon states. In this regime, transverse photonic AL has been observed using classical states of light [12, 9, 7, 11, 26]. Using such a random array, we study quantum walks using both$|\Psi_{\rm sep}\rangle$ and $|\Psi_{\rm EPR}\rangle$. (i) In the separable case [Fig. 3.3(a)] we observe for the first time AL at the single-photon level. Both photons in this separable state undergo independently the localization process (Fig. 3.3-ii-a and Fig. 3.3-iii-a). (ii) In the spatially entangled case, neither of the spatially extended EPR photons localizes (as observed

in the singles shown in Fig. 3.3-iii-b). In fact $G^{(2)}(x_1, x_2)$ in this regime resembles that of the input EPR state (Fig. 3.2-i-b). In other words, the spatial correlations inherent in $|\Psi_{\rm EPR}\rangle$ survive even in the presence of such extreme disorder. This two-photon disorder-mediated interference effect leads to localization in correlation space as seen clearly in the diagonal distribution (Fig. 3.3-iv-b). The exponential localization in the latter figure is evident from the linear slope (triangular shape) in the logarithmic scale we used in plotting. Whether this newly observed absence of diffusion in correlation space is a form of AL remains an open question. The hot-spotobserved in the data in Fig. 3.3-ii-b is due to the deviation between the assumed flat distribution of the random coupling coefficients in theory and the actual values in the fabricated sample.

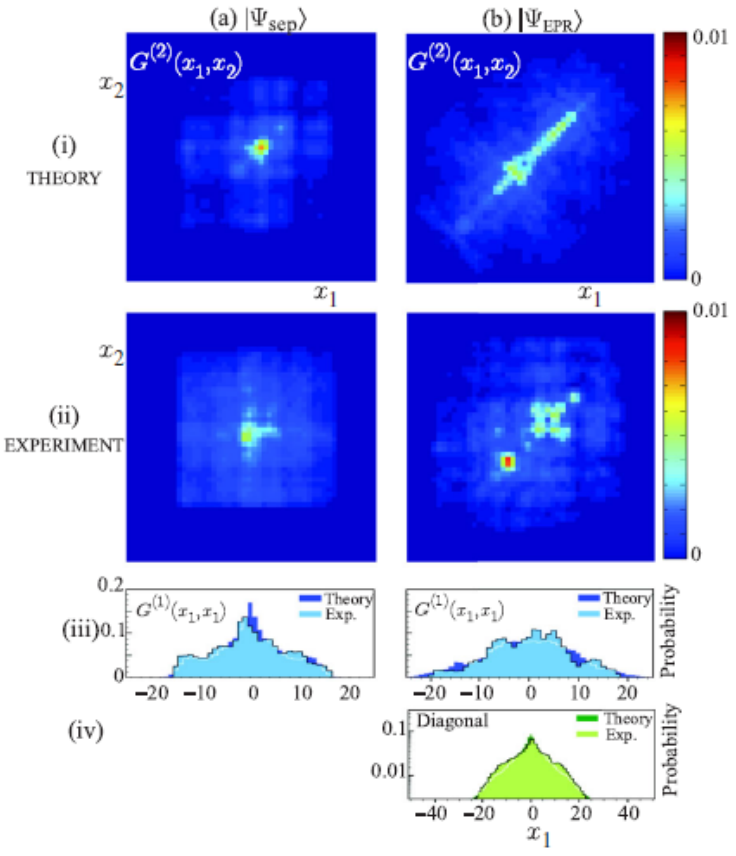

Figure 3.4: Same as in Fig. 3.2 for the weakly disordered Anderson lattice ($\Delta/\kappa_0 = 0.5$).

Weakly disordered array

We have also performed similar measurements in an array with coupling coefficients (Fig. 3.1-iii-b) chosen such that a one-photon state coupled into a single waveguide will exhibit an output distribution $G^{(1)}(x_1, x_1)$ that combines both ballistic propagation and AL features after propagating the physical distance L, but demonstrates a strong AL signature after twice the distance $2L$. The measurements of $G^{(2)}(x_1, x_2)$ for this array are shown in Fig. 3.4. For excitation in the state $|\Psi_{\rm sep}\rangle$, $G^{(2)}(x_1, x_2)$ does not localize as occurs in the case of the strongly disordered array [Fig. 3.3(a)]. The singles $G^{(1)}(x_1, x_1)$ in Fig. 3.4-iii-a reveal ballistic and AL features as is expected from the calculation of the evolution shown in Fig. 3.1-iv-b. When the photon pairs are coupled into 20 adjacent waveguides, and hence $|\Psi_{\rm EPR}\rangle$ is excited, the measured $G^{(2)}(x_1, x_2)$ is shown in Fig. 3.4-ii-b. The singles $G^{(1)}(x_1, x_1)$, Fig. 3.4-iii-b, reveal an extended distribution of both photons with no sign of localization. On the other hand, when the diagonals are examined (Fig. 3.4-iv-b, shown in logarithmic scale), we observe the localized state distribution that results from exciting a single waveguide in this array after propagating a distance $2L$, and hence exhibits a clear AL signature.

Conclusion

We have demonstrated deterministic and disordered quantum walks on large-scale on-chip lattices implemented on a spatially extended two-photon EPR state. Other entangled states besides $|\Psi_{\rm EPR}\rangle$ may also be launched into such multiport structures by manipulating the relative complex weights of the two-photon basis functions either at the NLC or using the imaging system. In the process, we observed AL at the single-photon level and also a new form of localization in correlation space resulting from the quantum random walk of an EPR photon pair on a disordered lattice. In principle, these systems may be adapted to incorporate other optical degrees of freedom, such as polarization and frequency, further expanding the dimensionality of the Hilbert space. Moreover, two dimen-

sional realizations of such networks, permanent or reconfigurable [52], can also be utilized for implementing more sophisticated operations and quantum random walks.

CHAPTER 4: ENTANGLED PHOTON PAIRS IN PHOTONIC LATTICES: PART II

Introductory Remarks on Experiment Three

The following paper is pre-press [15] and slated to be submitted to a peer-reviewed journal. As such, the paper as it is shown here may not be in its final published form. This paper continues and expands upon the work begun in the previous chapter. Here, I address through experiment and simulation the evolution of entangled photon pairs in disordered photonic lattices, where the entanglement is manifested through different types of correlations. The type of entanglement embodied by the photon pair is controlled by altering the input optical system. As before, if the input optical system is in an imaging configuration, photons generated at the same point in the crystal are imaged to the same point at the input face of the waveguide array, yielding a strongly correlated input state. Once this input state traverses the array, it again shows Anderson co-localization. In this case, I demonstrate AcL for a larger input state covering more waveguides and for more levels of disorder. If the input optical system is arranged in a $2-f$ Fourier transforming system, it is each photon's transverse momentum that determines which waveguide it enters, rather than its position. As such, each photon in the pair will enter a waveguide opposite a central point, yielding a spatially anti-correlated input state. The resulting $G^{(2)}(x_1, x_2)$ at the output reveals the phenomenon of Anderson anti-localization. The photons emerge from the array opposite or nearly opposite each other, again maintaining the correlations present in the input state. The localization signature is now revealed in the negative marginal, found by summing along the $x_1 = -x_2$ axis.

Next, I altered the correlations of the input state by modifying the input optical system. The extremes of imaging and Fourier transforming optical system produce input states with well defined

spatial correlations, where knowledge of the position of one photon absolutely gives the position of the other. Between these two extremes, the optical input system generates states in which the spatial correlations are not as extreme, but the two photons are still entangled. In these configurations, the entanglement is expressed via a combination of spatial and phase correlations. In my experiments, I show a transition between the extremes of correlated and anti-correlated input states and their corresponding output states by measuring the function $G^{(2)}(x_1, x_2)$. I observe the transition from Anderson anti-localization, to an intermediate state in with no strong spatial correlations, to an Anderson co-localized state.

Anderson Co-localization to Anti-localization of Entangled Photon Pairs in Disordered Photonic Lattices

Introduction

Quantum entanglement lies at the heart of a variety of fascinating phenomena and enables technologies that are beyond the bounds of classical physics. Quantum teleportation [53, 54], quantum computing [6] and secure quantum key distribution [4, 5] are a few of the profound and promising applications for which entanglement is essential. The degree and type of quantum entanglement present in a system is determined by measurement of multi-particle correlations in some degree of freedom. Interestingly, it has been shown that entanglement can migrate in the joint Hilbert space, causing entanglement to be expressed via correlations in a different degrees of freedom depending on how the particles have evolved [55, 56, 57].

Usually any non-intrinsic source of randomness or disorder is considered detrimental to fragile entangled systems. However, recent research into entanglement in disordered environments has revealed new and interesting physics that has potential far beyond mitigating undesirable effects.

For example, quantum random networks show markedly different properties than their classical counterparts [58], multiple scattering media may open new avenues for manipulating entangled states of light [59] and Anderson localization has been demonstrated for entangled photons in integrated photonic devices [60, 14]. Regarding the latter, experimental research into entangled photon propagation in disordered photonic systems has proven particularly fruitful, largely due to the ready source of entangled photon pairs through SPDC and advances in the fabrication of photonic lattices.

Photonic lattices are integrated multiport interferometers, consisting of arrays of waveguides in which light may evanescently couple from one waveguide to another. Due to their inherent customizability and stability, these devices serve as an ideal platform on which to test and demonstrate a variety of classical and quantum optical phenomena. In classical optics, they have been used to demonstrate transverse Anderson localization [7, 12, 8, 11] and study random walks of light [22]. In quantum optics, these arrays have been used to realize correlated quantum walks of photon pairs [50], and study non-classical correlations of photons in Anderson localizing media [27, 46]. We have previously used these arrays to demonstrate Anderson co-localization, a phenomenon in which two entangled photons localize in correlations space even though neither photon localizes on its own [14, 47].

In this report we investigate the spatial correlations of entangled photon pairs in Anderson localizing photonic lattices as entanglement of the input state is migrated between the extremes of correlation and anti-correlation. We begin by producing spatially entangled photon pairs via SPDC, then couple into a photonic lattice endowed with spatial disorder. We induce entanglement migration through the use of a fractional Fourier transform (fFT) [61, 62] optical system, which allows the entanglement of the photon pair to expressed jointly in spatial and phase correlations. After propagation through the array, the spatial correlations of the emerging photon pairs are measured via coincidence counting to recover the second order intensity correlation function $G^{(2)}(x_1, x_2)$.

In addition, we provide the first experimental evidence for Anderson anti-localization (AaL), in which photons pairs emerging from the array are anti-localized in correlation space.

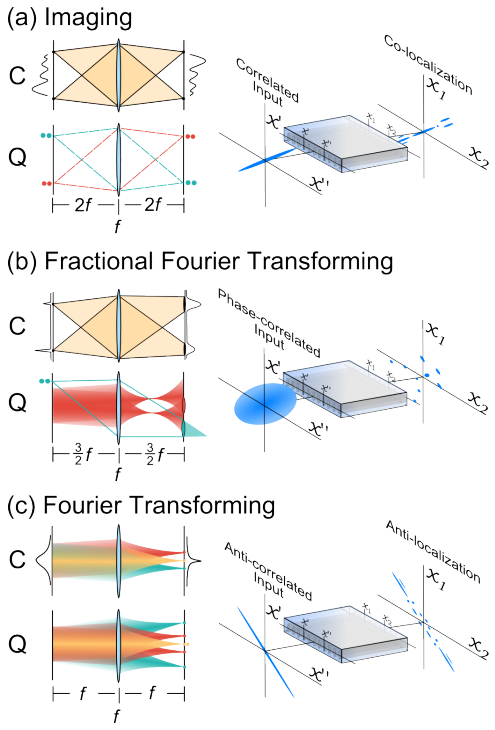

Figure 4.1: Schematic for input optical system in classical (C) and quantum (Q) regimes. The right column illustrates the evolution of the generated input states in the array. (a) (left) Imaging input configuration. (C) Each point in the object plane in imaged to a point in the image plane. (Q) A pair of photons created together in the NLC plane will be imaged to the same point at the input of the array, thus entering the same waveguide. (right) The correlated input evolves in the array and exits with the correlations largely intact, hence co-localization occurs. (b) (left) Fractional Fourier transform configuration. (C) A point in the object plane is a blur spot in the detection plane. (Q) Two photons created at the same point in the NLC plane are found within a certain distance of each other in the array input plane. Knowledge of the position of one photon does not yield complete information about the position of the other. Similarly, it will yield incomplete information about the possible transverse momentum of the photons. (right) The input state, which is neither fully correlated or anti-correlated (yet still fully entangled), evolves in the array and does not show any strong correlations at the exit of the array. (c) (left) Fourier transforming configuration. (C) Plane waves with different transverse momentum components are focused to different points in the detection plane. (Q) Photons in the pair generated by SPDC necessarily have opposite transverse momentum, such that they are always found in the detection plane on opposite sides of a central point. This results in an anti-correlated input state. (right) As the anti-correlated state evolves in the waveguide array, the anti-correlations are preserved, leading to AaL.

Theory

The propagation of light through a photonic waveguide array is characterized by the hermitian coupling matrix,

$$\mathbf{H} = \begin{pmatrix} \ddots & \ddots & 0 & \dots & 0 \\ \ddots & \beta_{n-1} & C_{n-1,n} & \ddots & \vdots \\ 0 & C_{n-1,n} & \beta_n & C_{n,n+1} & 0 \\ \vdots & \ddots & C_{n,n+1} & \beta_{n+1} & \ddots \\ 0 & \dots & 0 & \ddots & \ddots \end{pmatrix} \tag{4.1}$$

where β_n is the propagation constant of waveguide n, and $C_{n,n\pm1}$ is the coupling coefficient between adjacent waveguides n and $n \pm 1$, where $n = [-N, ..., -1, 0, 1, ..., N]$ is the position of the waveguide and $2N+1$ is the size of the array [44]. For an array of length L, elements of the matrix $e^{i\mathbf{H}L}$ determine the the discrete point spread function $h(x, x')$ of the linear system that relates the output at waveguide x to the input at waveguide x'. For waveguides with off-diagonal disorder, as used in our experiment, $\beta_n = \beta_o$ are fixed and $C_{n,n\pm1}$ are random parameters, so that the point spread function $h(x, x')$ has random components.

A single-photon wave function $\psi_i(x')$ at the input of the array generates a wave function

$$\psi_o(x_1) = \sum_x h(x_1, x')\psi_i(x') \tag{4.2}$$

at its output. For an initial wave function localized at $x' = 0$, i.e., $\psi_i(x') = \delta_{x',0}$, where $\delta_{x,0}$ is the Kronecker delta, $\psi_o(x) = h(x, 0)$. The probability of detecting the photon at waveguide x is then $\langle|\psi_o(x)|^2\rangle = \langle|h(x, 0)|^2\rangle$, where $\langle.\rangle$ represents the classical ensemble average. Conventional AL is exhibited since the width of this function is reduced as the level of disorder increases.

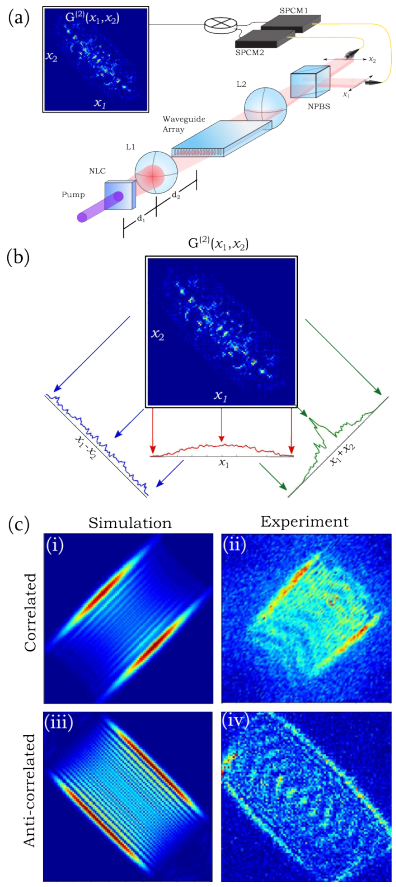

Figure 4.2: (a) Diagram of the experimental setup. From the left, a pump beam incident on a nonlinear crystal (NLC) produces spatially entangled photon pairs through type-I SPDC. A glan-thomposon polarizer (not pictured) removes the pump beam. A positive achromatic doublet (L1) couples the photon pairs to the waveguide array. The relation between d_1,d_2 and the focal length of L1 determines the type of spatial correlation embodied by the photon pair as it enters the array. After propagation through the array, the photons are imaged to a planes scanned by a pair of multimode fibers, separated by a nonpolarizing beamsplitter (NPBS). These fibers lead to a pair of single photon counting modules (SPCMs), which connect to a coincidence circuit. This enables us to produce the coincidence map $G^{(2)}(x_1, x_2)$. (b) A sample $G^{(2)}(x_1, x_2)$ showing how to derive the singles (red) and marginals M_+ (green) and M_- (blue) (c) Simulated (left) and measured (right) $G^{(2)}(x_1, x_2)$'s for periodic array when input is correlated (top) and anti-correlated (bottom).

Similarly, a two-photon wave function $\psi_i(x', x'')$ at the input of the array becomes

$$\psi_o(x_1, x_2) = \sum_{x', x''} h(x_1, x')h(x_2, x'')\psi_i(x', x'') \tag{4.3}$$

at the output. The probability of two-photon coincidence at positions x_1 and x_2 for light emerging from the array is $G^{(2)}(x_1, x_2) = \langle|\psi_o(x_1, x_2)|^2\rangle$. This is the quantity measured by our apparatus.

We are interested in the effect of the disordered medium on the spatial correlation of the initial function $\Psi_i(x', x'')$. The two special cases are fully correlated and fully anti-correlated, which are represented by $\Psi_i(x', x'') = \delta(x' - x'')$ and $\Psi_i(x', x'') = \delta(x' + x'')'$, respectively. These cases represent the cases of extreme spatial correlation, where knowledge of the position of photon one means knowing the position of photon two absolutely. In the correlated case, both photons will be found at the same waveguide site. In the anti-correlated case, the photons will be found in waveguides opposite a central point. In both cases, neither photon position is known before measurement, but their spatial correlations are strictly defined.

Between these two extremes, we have access to a continuum of intermediate input states in which the entanglement is expressed via a combination of spatial and phase correlations. Ideal versions of these states may be calculated by performing a fFT on the function $\Psi_i(x', x'') = \delta(x' - x'')$. Depending on the order fFT, the magnitude $|\Psi_i(x', x'')|$ may become separable, though the phase prevents the state itself from being separable. The implementation of the fFT is described in the experimental section and the method for simulating the non-ideal intermediate states is outlined in the supplement.

Experiment

Our experimental apparatus, shown in Fig. 4.2, consists of three parts: input state generation, the photonic waveguide array and coincidence measurement. A pump laser beam (vertically polarized, 403-nm, CW, 80-mW) is incident on a lithium iodate nonlinear crystal (NLC) (1.5-mm thick), cut to generate horizontally polarized, spatially entangled photon pairs via type-I spontaneous parametric down conversion. These photons are coupled to the input face of the waveguide array by a single positive lens of focal length $f = 30$-mm. The pump beam is removed by a polarizer. The specific configuration composed by the NLC, lens and input face of the array determines the type of spatial correlations embodied by the entangled photon pair. A $4f$ imaging system will yield spatially correlated photons, as photons created at the same point in the NLC are imaged to the same waveguide. A $2f$ Fourier transforming system will yield spatially anti-correlated photons, as the Fourier transforming lens translates the photons' opposing transverse momentum into position. Between the imaging and Fourier transforming systems, we have access to a continuum of states with a combination of spatial and phase correlations. In these cases, knowing the position of photon one yields a broad range of positions for photon two. In our experiments, we implement an optical FRFT via a balanced $(2\alpha)f$ optical system, where $1 \leq \alpha \leq 2$.

The waveguide arrays used in this experiment are inscribed in silica glass by use of femtosecond laser pulses [30]. Each array is made of 101 evanescently coupled, parallel, identical, single-mode, low-loss optical waveguides (width 4 μm, height 11 μm, NA 0.045, length L= 5 cm). In our work we consider four such arrays endowed with off-diagonal disorder. The disordered arrays are implemented by varying the separation between adjacent guides such that the coupling coefficients C_n are independent and uniformly distributed in the range $[C_o - \Delta, C_o + \Delta]$ with mean C_o and width 2Δ. The disorder level for our four disordered arrays are $\Delta C_o = 0.35, 0.51, 0.70, 0.87$.

After propagation through the array, the photons are imaged to the planes of a pair of scanning

multi-mode fibers (62.5-μm diameter) separated by a non-polarizing beam splitter. The magnification of this imaging system is such that the imaged height of each waveguide is matched to the diameter of the multi-mode fiber. The fibers, which are mounted to motorized linear stages, can be scanned and collect light from each waveguide independently. The fibers each lead to a single photon counting module, which are connected to a circuit that measures coincidence counts. In this way, we retrieve the coincidence map, or function $G^{(2)}(x_1, x_2)$.

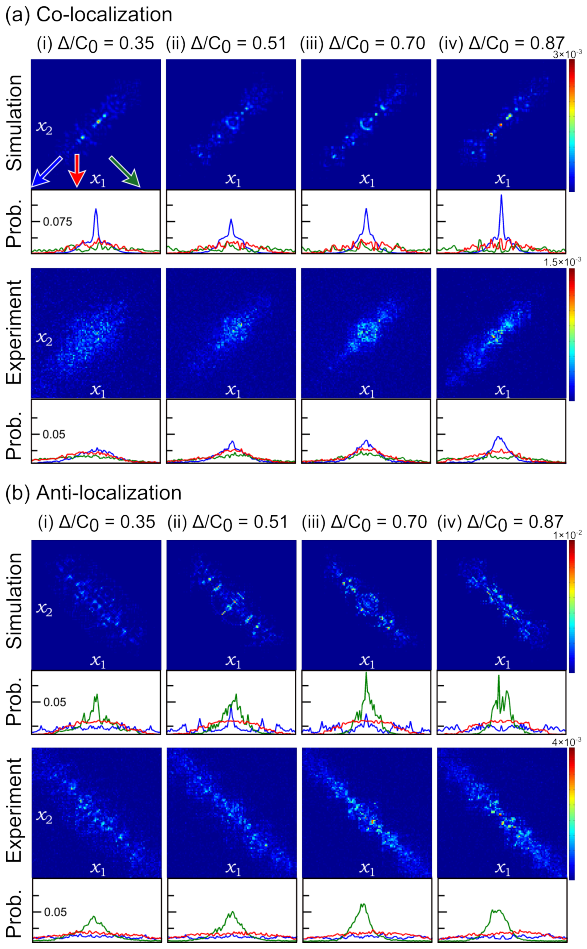

Figure 4.3: The simulated and observed correlation functions $G^{(2)}(x_1, x_2)$ at output of waveguide array for correlated and anti-correlated input states at various disorder levels. All of the coincidence maps span 100×100 waveguides. The inset graphs show the singles (blue) and marginals M_+(red) and M_- (green). The two rows in (a) correspond to input states that are spatially correlated, with the output coincidence maps demonstrating AcL. The two rows in (b) correspond to input states that are spatially anti-correlated and the output coincidence maps exhibit AaL.

Simulation

We have calculated the wave function $\psi_o(x_1, x_2)$ and its associated 2-photon coincidence function $G^{(2)}(x_1, x_2)$ at the output of the array for each of the disordered arrays used in the experiment, when

the wave function at the array input $\psi_i(x_1, x_2)$ is generated by the $4f$ and the $2f$ optical systems connecting the NLC to the array input. For degenerate, collinear SPDC and crystal thickness ℓ, the wave function $\psi(x_1, x_2)$ at the face of the NLC is the two-dimensional Fourier transform of the function

$$\Psi(q_1, q_2) = \int dq_p E(q_p)\xi(q_p, q_1, q_2)\delta(q_p - q_1 - q_2), \tag{4.4}$$

where $E(q_p)$ is the Fourier transform of the spatial profile of the pump beam electric field,

$$\begin{aligned} \xi(q_p, q_1, q_2) &= l\,\mathrm{sinc}\,(\ell\Delta k_z/2\pi)\exp(-i\ell\Delta k_z/2)\,, & (4.5)\\ \Delta k_z &= -\frac{\lambda}{2}\left(q_p^2/n_p - q_1^2/n - q_2^2/n\right), & (4.6) \end{aligned}$$

and n_p and n are the crystal refractive indexes at the pump and signal/idler wavelengths, respectively [63, 64].

For a perfect lens L1 with infinite aperture, the $4f$ configuration is a perfect imaging system, so that $\psi_i(x_1, x_2) = \psi(x_1, x_2)$. The $2f$ configuration implements a Fourier transform, so that

$$\psi_i(x_1, x_2) = \Psi(x_1/\lambda f, x_2/\lambda f), \tag{4.7}$$

where $\Psi(q_1, q_2)$ is given by Eq.(4.4).

Given $\psi_i(x_1, x_2)$, we have computed $\psi_o(x_1, x_2)$ by use of Eq.(4.3), where $h(x, x')$ are elements of the matrix $e^{i\mathbf{H}L}$, and $\mathbf{H}$ is given by Eq.(4.1).

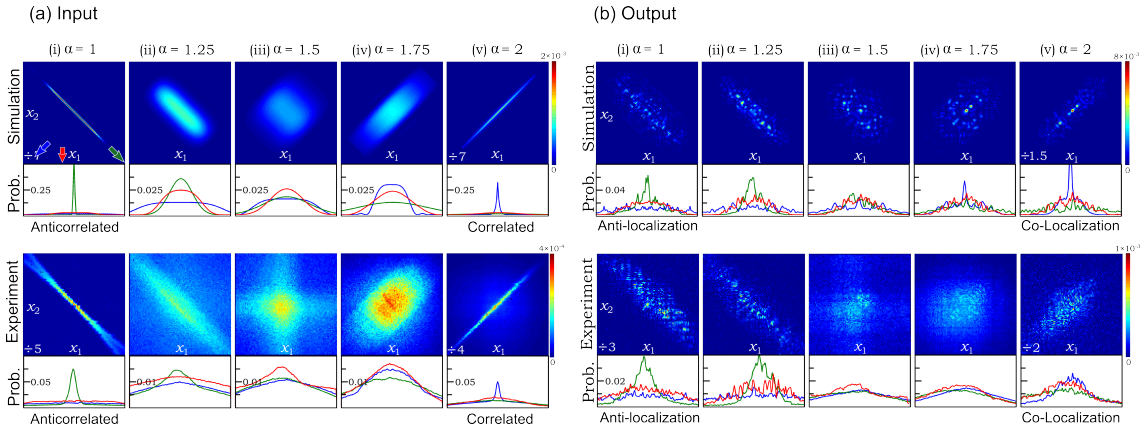

Figure 4.4: Simulated and observed coincidence maps showing a transition between anti-correlated and correlated two-photon states at the (a) input and (b) output of the disordered waveguide array. From left to right, the coincidence maps correspond to an optical input system in the $(2\alpha)f$ configuration, such that (i) corresponds to a Fourier transforming configuration and (v) corresponds to an imaging system. Due to space constraints the experiment row in part (a) was obtained using a lens with focal length of 6-cm. For these measurements, the pump beam diameter and the scanned range were doubled to compensate for the increased focal length; this setup is predicted to yield $G^{(2)}(x_1, x_2)$'s with nearly the exact same spatial correlations as the setup with f=3-cm.

Results

The experiment and simulation results are displayed in Figs. 4.3 and 4.4 in the form of coincidence maps $G^{(2)}(x_1, x_2)$. Each coincidence map is characterized by three one-dimensional projections given in the sideplots. The first is the singles distribution $S(x_2) = \sum_{x_1} G^{(2)}(x_1, x_2)$,which is the distribution of a single photon regardless of the other photon. The function $S(x_2)$ is proportional to the intensity distribution, and thus contains no information on the relationship between the photons. Projections along the diagonal and off-diagonal directions $x_2 = x_1$ and $x_2 = -x_1$ provide the marginal distributions functions $M_+(x_+) = \sum_x G^{(2)}(x, x_+ - x)$ and $M_-(x_-) = \sum_x G^{(2)}(x, x + x_-)$, which portray the two-photon correlation and anti-correlation, respectively. These three projections are useful tools for quantifying the type and strength of the two-photon spatial correlations.

For the spatially correlated initial two-photon wave function, the output photon coincidence maps and their projections are shown in Fig. 4.3(a,b), with the off-diagonal disorder increasing from $i - iv$. This input state is generated by imaging the plane of the NLC to the input face of the waveguide array. This entangled input state extends over about 70 waveguides, with both photons entering the same or nearby waveguides. Because of the extended nature of the input, the marginal distribution $S(x_2)$ remains extended and flat for all disorder levels, indicating that neither photon localizes on its own. However, as the disorder level increases the diagonal projection $M_+(x_+)$ is sharpened so that the coincidence distribution is localized along the $x_1 = x_2$ axis, meaning that while neither photon localizes on its own, the two photons will exit the array from the same or nearby waveguides. As predicted by the theory and simulation, the photon correlation present at the input of the array is preserved at its output in the presence of strong disorder. This confirms the AcL results obtained earlier in [14], though here we present results over more disorder levels and for an input state that covers significantly more waveguide sites.

Fully anti-correlated input states are generated by an $2f$ Fourier transforming input optical system; these input states correspond to the output coincidence maps shown in Fig. 4.3(c,d), with the disorder level increasing from $i - iv$. The Fourier transforming optical system translates each photon's transverse momentum to position. As each photon in the pair possesses opposite transverse momentum, the photons enter waveguides on opposite sides of the array, though which pair of waveguides is unknown. As the disorder level increases the projection $M_-(x_-)$ is sharpened so that the coincidence distribution is localized along the $x_1 = -x_2$ axis. Again, for all disorder levels the singles distribution $S(x_2)$ remains flat. As predicted by the theory and simulation, the photon anti-correlation present at the input of the array is preserved at its output in the presence of strong disorder; while neither photon localizes on its own, the photons are most likely to emerge on opposite sides of the central waveguide. This experimental result confirms for the first time the AaL predicted theoretically in [47].

The output coincidence maps for five input states, one correlated, one anti-correlated and three intermediate, are given in Fig. 4.4 (a,i-iv). From the simulation and input measurements prior to propagation through the array, a gradual transition between the anti-correlated and correlated cases is clearly observed. We note that even when there are almost no spatial correlations, the two photons remain fully entangled. In this case, the entanglement is expressed in the phase relations between the photons, rather than through their spatial correlations. We observe, in both the simulation and experiment, that the spatial correlations present at the input of the the array are again preserved by the disordered system.This is made especially clear by the distributions $M_+(x_+)$ and $M_-(x_-)$, which closely match for the input and output coincidence maps for the intermediate states.

Conclusion

We have used a set of disordered photonic waveguide array to provide experimental evidence for the assertion that strongly disordered photonic waveguide arrays that induce classical transverse Anderson localization preserve the spatial correlations of entangled, spatially extended two photon states. Initial two photon wavefunction initially confined to the sum/difference axis that are propagated through these disordered photonic waveguide arrays have their spatial correlations largely preserved, phenomena we term Anderson co-localization (AcL) and Anderson anti-co-localization (AaL). In this report, we provide the first experimental evidence for AaL. In addition, we have provided evidence that even when the spatial correlations are not localized on the sum or difference coordinate, as with states generated by an optical system that performs a fractional Fourier transform, the type and strength of the spatial correlation present at the input of the array is preserved in the output coincidence map.

The great appeal and surprise of AL is that a counterintuitive effect, disorder in a system leading to

localization instead of accelerated diffusion, arises out of a simple model with simple assumptions, and yet is applicable in fields far outside its original scope. Although our experiments and analysis are currently confined to a designed and manufactured photonic device, we believe that the fundamental ideas espoused here may be applicable to variety of areas in which quantum particles interact with disordered systems. This is particularly important as new techniques and technologies seek to take advantage of multi-particle quantum interference effects in complex systems or networks.

Supplementary

Two-Photon State at Nonlinear Crystal

The two photon state at the nonlinear crystal (NLC), prior to any propagation, is given in terms of the transverse momentum by the following equation:

$$\Psi^{(2)}(q_1, q_2) = \int dq_p E(q_p)\xi(q_p, q_1, q_2)\delta(q_p - q_1 - q_2), \tag{4.8}$$

where $E(q_p)$ is the Fourier transform of the spatial profile of the pump beam, $\xi(q_p, q_1, q_2)$ is the longitudinal phase matching condition and the delta function indicated perfect phase matching in the transverse direction. The phase matching function $\xi(q_p, q_q, q_2)$ is given by:

$$\xi(q_p, q_1, q_2) = \text{sinc}\left(\ell\Delta k_z/2\pi\right)\exp(-i\ell\Delta k_z/2)\,, \tag{4.9}$$

where l is the longitudinal thickness of the NLC and Δk_z, the longitudinal component of the the

wavevector, is:

$$\Delta k_z = \sqrt{\frac{n_p^2}{\lambda_p^2} - q_p^2} - \sqrt{\frac{n_1^2}{\lambda_1^2} - q_1^2} - \sqrt{\frac{n_2^2}{\lambda_2^2} - q_2^2}. \tag{4.10}$$

Equation 4.10 may be simplified by applying the paraxial approximation terms in the square roots, assuming the generated photons are degenerate in wavelength ($2\lambda_p = \lambda_1 = \lambda_2$) and assuming the generated photons are collinear ($n_p = n_1 = n_2$). This results in the following:

$$\Delta k_z = -\frac{\lambda}{2}\left(q_p^2/n_p - q_1^2/n - q_2^2/n\right). \tag{4.11}$$

Combining equations 4.8, 4.9 and 4.11 yields the two-photon state at the NLC in terms of the transverse momentum of each photon. The Fourier transform of this quantity yields the state equation in terms of the position of each photon. For a thin NLC, the two photons will always be found at the same location as they are created at the same point in the NLC.

Propagation from NLC plane to array plane

A single photon in the state $\psi_i^{(1)}(x')$ will evolve according to the following equation:

$$\psi_o^{(1)}(x_i) = \int dx h(x_i, x_1)\psi_i^{(1)}(x_1), \tag{4.12}$$

where $h(x_1, x')$ is the impulse response function corresponding to propagation from the plane x' to x_1. In our experiments, the photons each propagate in the same environment. We may then determine how the two-photon state $\psi_i^{(2)}(x', x'')$ evolves using the same impulse response function

for each photon:

$$\psi_o^{(2)}(x_i, x_s) = \int dx_1\ dx_2 h(x_i, x_1) h(x_s, x_2) \psi_i^{(2)}(x_1, x_2). \tag{4.13}$$

We may write a similar equation for evolving the state in terms of the transverse momentum instead of the spatial coordinate:

$$\psi_o^{(2)}(x_i, x_s) = \int dq_1\ dq_2 H(x_i, q_1) H(x_s, q_2) \psi_i^{(2)}(q_1, q_2). \tag{4.14}$$

The impulse response functions $h(x, x')$ and $H(x, q)$ are related through the Fourier transform,

$$H_i(x_i, q_1) = \int dx_1 h(x_1, x_i) \exp(-i q_1 x_1)\,. \tag{4.15}$$

We explore three simple optical configuration consisting of a single lens: an imaging system, a Fourier transforming system and an intermediate system. The spatial impulse response function for evolving a single photon through the system in Fig. (A1) is, assuming an infinite lens aperture, given by the following equation:

$$\begin{aligned} h_i(x_i, x_1) = A \exp\left[i \frac{k_i}{2} \left(\frac{x_i^2}{z_1} + \frac{x_1^2}{z_2} \right) \right] \\ \times \int_\infty^\infty dx \exp\left[i \frac{k_i}{2} \left(\frac{1}{z_1} + \frac{1}{z_2} - \frac{1}{f} \right) x^2 - i k_i \left(\frac{x_1}{z_2} + \frac{x_i}{z_1} \right) x \right] \end{aligned} \tag{4.16}$$

Fourier Transforming Configuration

If the input plane, lens and output plane are in a Fourier transforming configuration ($z_1 = z_2 = f$), evaluating the integral in equation 4.16 and Fourier transforming the result according to equation 4.15 yields:

$$H_i(x_i, q_1) = A\,\delta\left(\frac{2\pi x_i}{\lambda f} - q_1\right). \tag{4.17}$$

This is the expected result, as it indicates a plane wave with transverse momentum q in the object plane becomes a point at position $x = \frac{\lambda f q}{2\pi}$ in the Fourier plane.

Imaging Configuration

If the input plane, lens and output plane are in an imaging configuration ($\frac{1}{z_1} + \frac{1}{z_2} = \frac{1}{f}$), evaluating the integral in equation 4.16 and Fourier transforming the result according to equation 4.15 yields:

$$H_i(x_i, q_1) = A\ \exp\left[i\frac{\pi x_i^2}{\lambda z_2}\left(1 + \frac{z_1}{z_2}\right)\right] \exp\left[i\frac{z_1}{z_2}x_i q_1\right]. \tag{4.18}$$

This equation is a Fourier transform accompanied by a quadratic phase factor. In most treatments this phase factor is neglected; however, in our experiments we are coupling the two-photon state into a multiport interferometric device, meaning the additional phase should be accounted for.

Intermediate Input Configuration

Lastly, if the input optical configuration is neither imaging nor Fourier transforming, but an intermediate state ($z_1 = z_2 < f$), equations 4.16 and 4.15 yield the equation:

$$H_i(x_i, q_1) = A \left[\frac{i\pi}{z_1 \lambda_i} \left(1 - \frac{\Delta}{z_1} \right) \right]^{-\frac{1}{2}} \exp\left[i\Lambda_1 x_i^2 \right] \exp\left[-i\Lambda_2 q_1^2 \right] \exp\left[i\Lambda_3 x_i q_1 \right], \tag{4.19}$$

where $\Delta = \frac{1}{f} - \frac{1}{z_2} - \frac{1}{z_1}$ and

$$\Lambda_1 = \frac{\pi}{\lambda_i z_1} \left[1 - \frac{\Delta}{z_2} - \frac{\Delta^2}{z_2(z_1 - \Delta)} \right]; \Lambda_2 = \frac{z_1 \lambda_i}{4\pi \left(1 - \frac{\Delta}{z_1} \right)}; \Lambda_3 = \frac{\Delta}{z_2 \left(1 - \frac{\Delta}{z_1} \right)}. \tag{4.20}$$

Propagation through the Array

Once the state at the face of the waveguide array is known, it can be discretized and propagated through the array. In our experiments, we judged that the wave function fluctuates slowly over the size of our waveguide array, and thus the discretization procedure consists only of sampling from the continuous field at the appropriate locations. The two photon state may then be evolved through the array by use of the discrete analogy of equation 4.13. The discrete impulse response function $h_{x,x'}$ for a given propagation distance L is simply the elements of the evolution operator $\mathbf{U} = \exp(-i\mathbf{H}L)$, where $\mathbf{H}$ is the coupling matrix given in the paper.

CHAPTER 5: SPATIAL FREQUENCY IN PHOTONIC LATTICES

Introductory Remarks on Experiment Four

The following paper is pre-press [65] and slated to be submitted to a peer-reviewed journal. As such, the paper as it is shown here may not be in its final published form. In this chapter, I address, through simulation and experiment, the action of the periodic and disordered photonic lattices in terms of spatial frequency (SF). Photonic lattices have been extensively studied and used to show novel phenomena in discrete optics and photonic analogies of phenomena from different fields. However, very limited work has been done on how photonic lattices affect the spatial frequency spectrum of light. Here, I examine the spatial and SF impulse response functions of the periodic and disordered arrays, uncovering surprising results.

First, I overview the theory of classical light propagation in one dimensional photonic lattices using impulse response functions and show how one may evolve the electric field in terms of spatial frequencies instead of the spatial distribution. I then show the relation between the spatial frequency of the electric field and a plane wave incidence on the array from a given angle. Using this understanding, I elaborate on how the various impulse response functions can be measured in the experiment. In the periodic arrays, I find that the impulse response function that links a spatial impulse input and a spatial frequency output has an intricate structure in areas where the array must be considered spatially invariant.

In the disordered arrays, I find the surprising results that spatial frequency inputs (plane waves with a given transverse momentum) are not completely scrambled as they evolve in the disordered waveguide arrays. Instead the plane wave is broken into two components with the same magnitude but opposite sign, similar to reflection and transmission. This effects leads to a spatial frequency

impulse response function that has an X-shape. This result illustrates the very different nature of light propagation is discrete vs. continuous random media.

Spatial Frequency in Periodic and Anderson Disordered Photonic Lattices

Introduction

Photonic lattices, which are arrays of evanescently coupled waveguides, are well studied and powerful tools for the study of novel phenomena in linear and nonlinear discrete optics. These devices are integrated, customizable multi-port interferometers that allow for extremely precise control of the flow of light. Photonic lattices can be designed to realize optical analogies of phenomena native to other physics systems [66], such as quantum walks [22], Anderson localization [12, 9, 11] and Bloch waves [19, 20]. In this report, we investigate the spatial frequency (SF) spectrum of periodic and Anderson disordered photonic lattices and uncover some surprising insights.

We briefly review the theory governing the propagation of light in one-dimensional photonic lattices and how each it be characterized by the discrete, spatial impulse response function (IRF). We show how these equations may be recast in terms of SF and explore their structure for both the periodic and disordered arrays. As we examine each IRF, we discuss how the array does or does not alter the input SF spectrum. We culminate this report by revealing the unexpected shape of the IRF that relates the input and output SF for disordered photonic lattices; we find that instead of scrambling the input SF as might be expected by propagation in a highly disordered medium, the input light is split into two components with equal SF magnitude, but opposite sign. This result reinforces the dramatic difference between light propagation in discrete and continuous random media.

Theory

Given an input electric field E_x, the electric field $E_{x'}$ at the output plane of a discrete linear optical system may be determined though use of the discrete spatial impulse response function $h_{x',x}$ as follows:

$$E_{x'} = \sum_{x} h_{x',x} E_x. \tag{5.1}$$

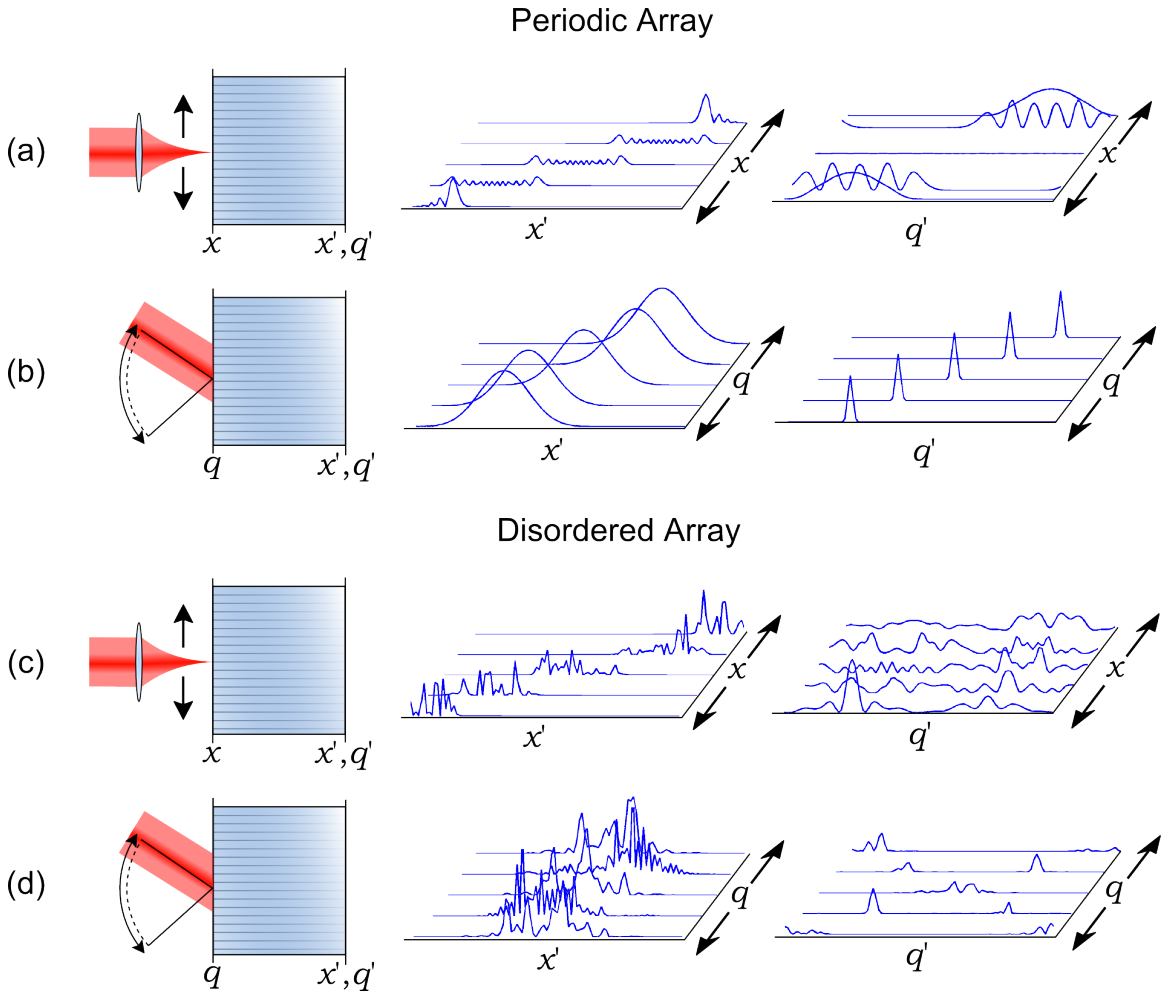

Figure 5.1: Schematic demonstrating the method of measuring the various impulse response functions (left column) and simulations of the corresponding results for a set of inputs. The results are shown for the (a-b) periodic and (c-d) weakly disordered regimes. The features of these graphs are discussed extensively in the text.

We will consistently use the prime notation to designate the output plane. In photonic waveguide arrays, the calculation of $h_{x',x}$ is straightforward. The propagation of light in a photonic waveguide array with N waveguides and only nearest neighbor coupling is governed by a set of N linear

differential equations

$$i\frac{dE_n}{dz} = \beta_n E_n + C_{n,n-1}E_{n-1} + C_{n,n+1}E_{n+1} \tag{5.2}$$

where E_n is the electric field in waveguide n, β_n is the propagation constant for waveguide n, and $C_{n,n\pm1}$ is the coupling constant between waveguide n and $n \pm 1$. Rewriting this set of equations in matrix form yields

$$\frac{d}{dz}\left[\mathbf{E}\right] = -i\left[\mathbf{H}\right]\left[\mathbf{E}\right] \tag{5.3}$$

where the coupling matrix $[\mathbf{H}]$ is written in terms of the parameters of the lattice, as follows:

$$\left[\mathbf{H}\right] = \begin{pmatrix} \ddots & \ddots & 0 & \dots & 0 \\ \ddots & \beta_{n-1} & C_{n-1,n} & \ddots & \vdots \\ 0 & C_{n-1,n} & \beta_n & C_{n,n+1} & 0 \\ \vdots & \ddots & C_{n,n+1} & \beta_{n+1} & \ddots \\ 0 & \dots & 0 & \ddots & \ddots \end{pmatrix}. \tag{5.4}$$

The solution to this differential matrix equation is $[\mathbf{E}] = e^{-i[\mathbf{H}]z}\left[\mathbf{E}(0)\right]$. Comparing this solution to Eqn. 5.1 reveals $h_{x',x} = \left[e^{-i[\mathbf{H}]z}\right]_{x',x}$.

It follows that any initial electric field defined at each waveguide $n \in N$ may be propagated a distance z for any array defined by Eqn. 5.2. The simplest case is a periodic array with an infinite number of waveguides, in which each waveguide has identical propagation constants and coupling coefficients. The impulse response function $h_{x',x} = i^{x-x'}J_{x-x'}(2Cz)$, where J_l is l^{th} order Bessel

function of the first kind. If $E(z=0) = \delta_{x,n}$, i.e. light is coupled into a single waveguide n, the output intensity distribution will be $I(x') = |J_{x'-n}(2Cz)|^2$, with most of the energy confined to two ballistic lobes. The distance between these lobes increases linearly with Cz.

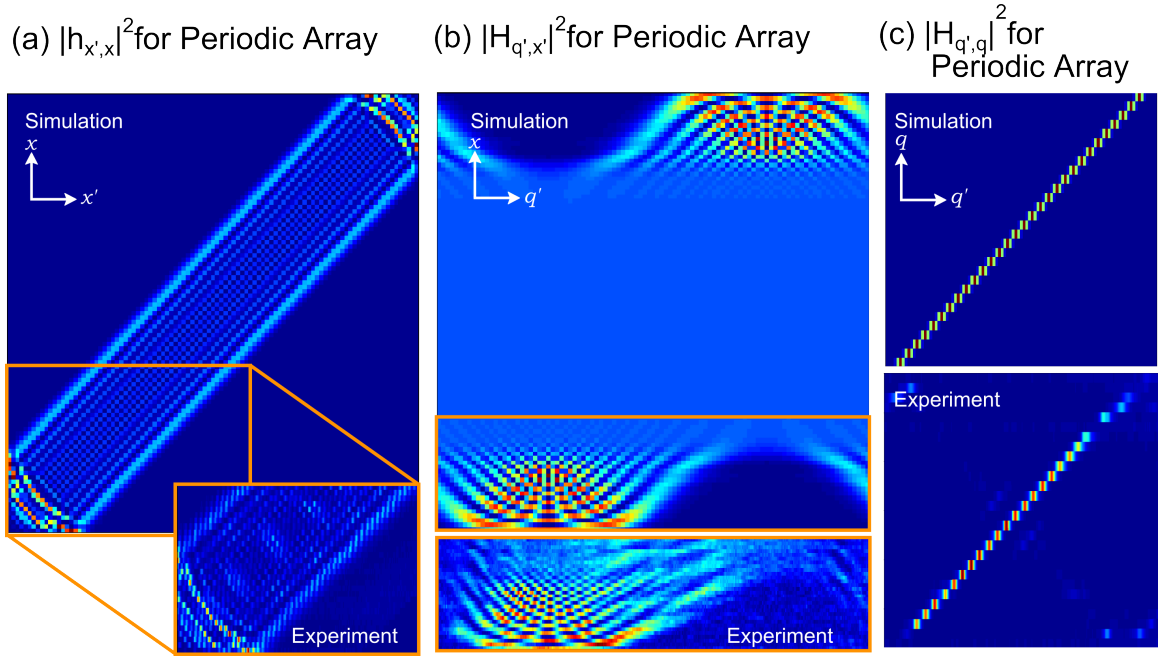

Figure 5.2: Simulations and experimental results corresponding to the periodic photonic lattice. (a) Color plots of $|h_{x'x}|^2$ from simulation (top) and experiment (bottom). In this experiment, light is coupled into a single waveguide at a time and the intensity at the output is directly recorded. The input waveguide is shifted and the process repeated. The final results are then compiled and plotted. (b) Color plots of $|H_{x,q'}|^2$ from simulation (top) and experiment (bottom). Here, light is coupled into a single waveguide and the output is Fourier transformed. In this plot, the primary interest is when the input is near the edge of the array and reflections can occur, as the Fourier transform of the unreflected Bessel function yields a uniform intensity distribution. (c) Color plots of $|H_{q,q'}|^2$ from simulation (top) and experiment (bottom). Here, a plane wave input at some angle corresponding to spatial frequency q traverses the array and its intensity in the Fourier plane is measured. For the periodic array this results in a single focused point whose position is proportional to q.

We also consider the case of off-diagonal disorder, in which either the coupling coefficients are selected from a uniform random distribution in a range $C = C_0 \pm \Delta$. At high disorder levels, the ballistic propagation characteristic of the periodic array is fully arrested and, upon averaging over

many realizations of disorder, transverse Anderson localization is observed. Anderson localization in photonic lattices has been extensively studied.

In this treatment we have thus far consider the action of the array in the spatial basis. This is the natural course, as Eqn. 5.2 can be written compactly and directly in terms of the propagation constants and coupling coefficients. Of course, the electric field in the array may also be defined in terms the transverse momentum or spatial frequency (SF). One may translate between the spatial and SF bases through the discrete Fourier transform, yielding the new equation of propagation $[\mathbf{E_q}] = \mathbf{U_q}(z)\,[\mathbf{E_q}(0)]$, where $\mathbf{U_q}(z) = \mathbf{D}e^{-i[\mathbf{H}]z}\mathbf{D}^{\dagger}$ and $\mathbf{D}$ is the discrete Fourier transform operator. With this in mind, we rewrite eqn. 5.1 for SF as

$$E_{q'} = \sum_{q} H_{q',q} E_q. \tag{5.5}$$

Whereas $h_{x',n}$ describes how an electric field originating at a single waveguide n evolves in the lattice, its SF counterpart $H_{q',k}$ describes the propagation of an electric field $E_q = \delta_{q,k}$ with uniform amplitude in every waveguide and a constant phase difference, proportional to k, between neighboring waveguides. In an experimental setting, such an electric field corresponds to a plane wave traveling at some angle θ relative to the optic axis. The distance between the waveguide arrays, θ and the wavelength of the plane wave determine the SF E_q.

Additionally, we may define hybrid impulse response functions that relate the SF input to a spatial output ($H_{q',x}$) or vice versa ($H_{x',q}$). Heretofore photonic lattices have not been examined from this SF perspective. The exception is the magnitude square of the hybrid impulse response function $H_{x',q}$, which has been experimentally observed for periodic lattices [18], as it has interesting properties related to the band structure of the array.

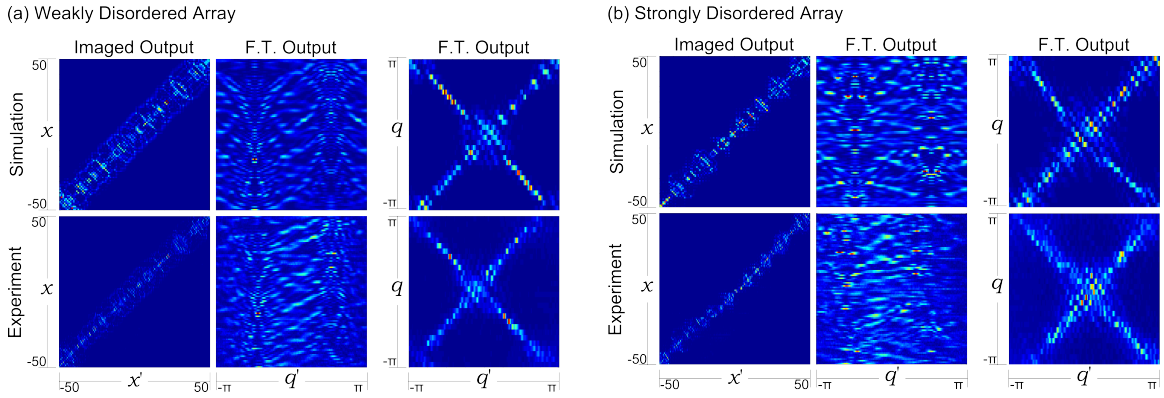

Figure 5.3: Simulated and experimental results for the (a) weakly disordered and (b) strongly disordered photonic lattices. Each set shows, from left to right, the functions $|h_{x',x}|^2$, $|H_{q',x}|^2$ and $H_{q,q'}$.

Periodic Array

The experimental procedure for obtaining the magnitude squared of the impulse response functions is straightforward and illustrated in Fig. 5.1. We note that the complexed valued impulse response function cannot be obtained without phase measurements, as only the intensity, and not the field, can be measured. As shown there are four impulse response functions (for each photonic lattice) that may be obtained. In Fig. 5.1-(a), a spatial impulse $E_x(z=0) = \delta_{x,n}$ is generated at the input, i.e., light is coupled into a single waveguide located at $x = n$. This impulse, according to equation 5.1, evolves to $E_{x'} = h_{x',n}$, with corresponding intensity $I_{x'} \propto |h_{x',n}|^2$. This means the measured intensity is a lateral slice of the function $|h_{x,x}|^2$ that we wish to recover; five of these slices for different n are shown in the left plot of Fig. 5.1-(a). For the inputs far from the array edges, the intensity distribution is the Bessel function described earlier. Closer to the edges, reflections from the edges of the array lead to more complicated distributions that have been studied in [26]. The full simulation and experimental results are shown in Fig. 5.2-(a) and show excellent agreement.

To obtain the hybrid impulse response function $|H_{q',x}|^2$ we take the Fourier transform of the field

$E_{x'} = h_{x',n}$ with respect to the output coordinate x', which in the experiment is implemented by an optical Fourier transforming lens between the output face of the photonic lattice and the detection plane. The measured intensity distribution is now a lateral slice of $|H_{q',x}|^2$. When the input waveguide n is far from the edges, the intensity distribution is uniform in the Fourier plane, as indicated by middle slice of $|H_{q',x}|^2$ in Fig. 5.1-(a). In this region, the periodic array is locally shift invariant, and thus cannot alter the SF spectrum of the input state. As a spatial impulse $E_x = \delta_{x',n}$ at the input contains the full SF spectrum uniformly, the SF at the output is also necessarily uniform. Once the input waveguide is close enough to the edge of the array for reflections to occur, the array is shift invariant, and a finely detailed structure is observed in the detection plane. The full result can be seen is Fig. 5.2-(b), which shows simulation and measurement.

The previous two impulse response functions relate a spatial impulse input to spatial and SF outputs; the next two, illustrated in Fig. 5.1-(b), relate a SF impulse input to the spatial and SF outputs. As mentioned above, the SF impulse is experimentally generated by a plane wave coupled uniformly into all the waveguides at some angle, so as to produce a constant phase step between neighboring waveguides. As shown in the drawing, varying the input direction of the beam varies q. In our experiments, we approximate the plane wave with a broad Gaussian beam covering most of the array. Thus, the resulting measured intensity distribution is only an approximation of the impulse response function corresponding to the set of illuminated waveguides. The left plot of Fig. 5.1-(b) shows the spatial intensity distribution for varying plane wave inputs. We do not reproduce this result in the experiment, as it has been well studied. It was shown that Gaussian input beams may, at certain spatial frequencies, traverse the array without diffracting [67].

The SF distribution for varying plane wave inputs, however, has not been previously examined. As can be seen in the right plot of Fig. 5.1-(b), the broad Gaussian beam is Fourier transformed into a single, tightly focused Gaussian peak that translates across the Fourier plane as the input angle is varied. Again, if we consider the array to be shift invariant over the illuminated section of

waveguides, the SF spectrum of the input is not altered. The output in the Fourier plane is thus a sharp peak at a position proportional to the input SF q, forming a diagonal line on the $q = q'$ axis. The simulation and experimental results are shown in Fig. 5.2-(c). In the experimental results, we attribute the small amount of signal off the diagonal to reflections from the edge of the array.

Disordered Arrays

The impulse response functions for the disordered array are wholly different. In left plot of Fig. 5.1-(c), we see the ballistic diffraction present in the periodic array is arrested and the intensity distribution begins to localize. This onset of transverse Anderson localization has been theoretically and experimentally studied in other works [8, 9, 11, 12]. In the right graph, the Fourier transform does not appear to have a definite structure. However, referencing the graphs $|H_{q',x}|^2$ in Fig. 5.3, we observe for both disordered arrays, points with higher intensity tend fall on or near the lines where $q = \pm\frac{\pi}{2}$. These spatial frequencies are of special importance; when light travels from a waveguide to its neighbor it will acquire a phase shift of $\pm\frac{\pi}{2}$, depending on the separation between the waveguides. It is also at these spatial frequencies that Gaussian beams traverse the periodic array without diffraction [67]. The full simulations and experimental results for $|h_{x',x}|$ and $|H_{q',x}|^2$ are shown in Fig. 5.3 for the (a) weakly and (b) strongly disordered arrays. We note particularly good agreement between simulation and experiment for the weakly disordered array.

The plots in Fig. 5.1-(d) show lateral slices of the functions (left) $|H_{x',q}|^2$ and (right) $|H_{q',q}|^2$ for selected values of q. The impulse response function $H_{x',q}$, which is not measured in our experiment, shows an intensity profile with broad envelope and random peaks. This result is expected, as any diffraction that might take place is halted by the disorder in the array. As in the periodic array, this result was not experimentally measured.

Finally, we come to the most surprising result of this report, the structure of $|H_{q',q}|^2$. It might be

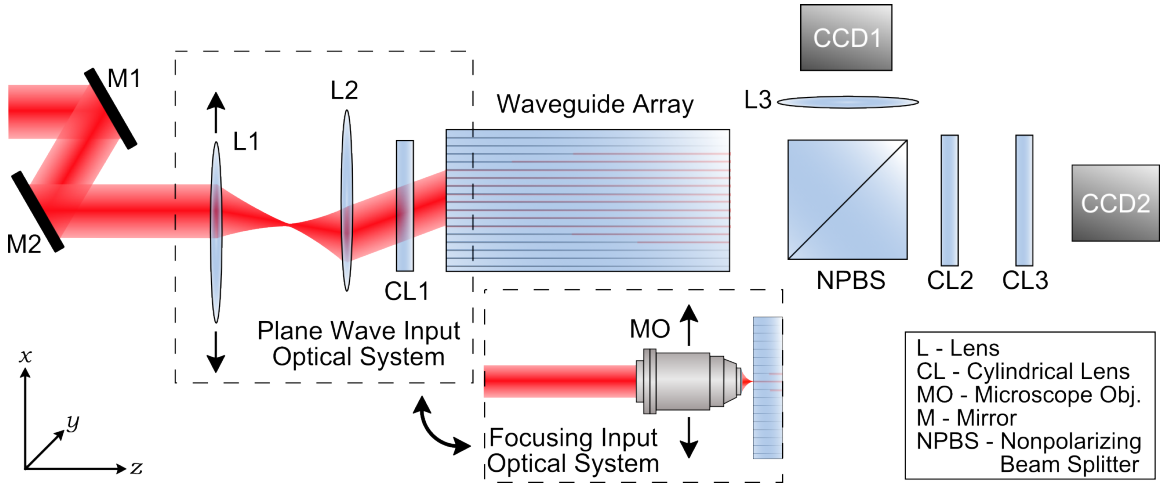

Figure 5.4: Diagram of the experimental setup with two types of inputs (point and plane wave) and the ability to measure the output intensity and the Fourier transform in concert. Details of the setup are in the text.

expected that, in the disordered array, the initial SF q of a plane wave or broad Gaussian input would be completely obscured by the highly disordered medium. However, we find that the SF spectrum at the output of the array is confined to peaks centered at the values of $\pm q$. When multiple input q's are scanned over, the resulting $|H_{q',q}|^2$ is seen to have an X-shape, which is shown in its entirety in Fig. 5.3. If we consider the SF to be the direction of a plane wave, we see from this plot that the disordered array breaks the incoming beam into transmitted and reflected components. The simulation and results, plotted in the rightmost columns in Fig. 5.3 (a) and (b), show good agreement and verify this surprising result.

Experiment

The experimental setup is shown in Fig. 5.4. The measurements performed with this system allow us to recover absolute value squared of the spatial and SF impulse response functions, i.e. $|h_{x,x'}|^2$, $|H_{x,q'}|^2$ and $|H_{q,q'}|^2$. The setup has two input configurations. In both, a laser beam (780-nm

collimated LightPath fiber laser) enters from the left and reflects off two alignment mirrors M1 and M2. For the plane wave input configuration, the laser is passed through two lenses L1 and L2 with focal lengths f_1 and f_2, respectively, that are a distance $d = f_1 + f_2$ apart. This setup simply works as a beam expander/compressor when L1 and L2 are aligned along the optic axis. In our setup, we move L1 in the x-direction to induce a tilt in the beam after L2. In this way, we control the angle at which the beam impinges upon the waveguide array, effectively selecting different values of q. After L2, but before the array, the laser is focused in the y-direction a cylindrical lens CL1. This is to maximize the light that is coupled into the waveguides. For the single waveguide input, the laser is simply coupled into a single waveguide via a microscope objective (30x). Then the waveguide array may be translated in the x-direction to couple into different waveguides.

The waveguide array itself was made by femtosecond laser pulses focused into a glass substrate, as prescribed by Szameit et. al. [30]. The array is made up of identical, parallel waveguides. Each set is composed of 101 waveguides; disorder is induced by varying the intra-waveguide spacing, which alters the coupling coefficients between waveguides. In this experiment, we use three different arrays: periodic, weakly disordered ($\Delta/C_0 = 0.4$), and strongly disordered ($\Delta/C_o = 0.9$).After propagation through the array, the light travels through a non-polarizing beam splitter (NPBS). In the reflected direction, the lens L3 ($f = 4$-cm) images the output face of the array to CCD1 and the image is recorded; the intensity at the output of every waveguide can then be obtained via simple image processing. In the transmitted direction, a cylindrical lens CL2 ($f = 4$-cm) images the output face of the waveguide array in the y-direction, while CL3 ($f = 10$-cm) performs a Fourier transform in the x-direction. The result is recorded by CCD2. In both cases, imaging processing is used to extract the intensity distributions by vertically integrating a small number of pixels spanning the area of interest.

Conclusion

In this report we have examined periodic and Anderson disordered photonic lattices in the spatial and SF regimes through both simulation and experiment. We have demonstrated the unexpected effects that arise when considering the SF component, such as the detailed structure of $|H_{q',x}|^2$ and the X-shape of $|H_{q',q}|^2$. Though photonic lattices have been used extensively to study novel optical phenomena, we are the first to elucidate the action of one dimensional periodic and disordered arrays in terms of SF. In this report, we utilized two of the simplest realizations of these devices; many other configurations have been designed and used to demonstrate a wide variety of effects. It is our hope that this work will lead to the exploration of SF spectrum for related devices and the discovery of more interested optical phenomena.

CHAPTER 6: CONCLUSION

In this dissertation I have, through the papers pre-published and republished here, reviewed the research I have performed as a part of the Quantum Optics Group in the College of Optics and Photonics at the University of Central Florida. In the course of my research, I have utilized photonic waveguide arrays for the study of classical and quantum light when the equations governing its evolution are discretized. This work is of fundamental and practical importance. Firstly, discrete optics in general is a fascinating field full of rich physics. There is a dramatic difference between the propagation of light in continuous and discrete systems, such that even diffraction occurs in an unfamiliar and interesting way. Secondly, thanks to major advancements in fabrication techniques, these devices are highly customizable and can be tailored to mimic a host of novel phenomena from many areas of physics. They are essentially a toy model that can be utilized for exploring complicated effects from other disciplines or creating entirely new phenomena. When these interesting devices are used in conjunction with quantum light, it opens up a whole new area of physics and optics to explore. In this dissertation, I have reviewed the research I have performed on periodic and disordered photonic waveguide arrays in both the classical and quantum regimes. I have explored their use in modeling effects from other fields and discovered entirely new effects in both classical and quantum discrete optics.

In the first paper [9], I demonstrated through both numerical simulation and experiment the transition from ballistic propagation to transverse Anderson localization in off-diagonal disordered waveguide arrays. This was the first time Anderson localization has been shown in waveguide arrays with off-diagonal disorder. In addition, we demonstrated through simulation the equivalence of shifting the array then averaging and averaging over independent realizations of disorder.

The the second paper [14] I reported, through simulation and experiment, the propagation of spa-

tially extended, entangled photon pairs in both the periodic and disordered photonic waveguide arrays. In this experiment, I generated entangled photon pairs through spontaneous parametric down conversion and imaged them to the input face of the waveguide array, meaning the photons entered the same waveguide, but which waveguide was unknown. After propagation in the array, the positions of each photon pair were measured in coincidence, allowing the generation of the coincidence map. In the course of this research, I experimentally verified the phenomenon of Anderson co-localization, in which the entangled photon pair, initially spatially correlated, traverses the disordered array and localizes in correlation space, even though neither photon localizes on its own. The signal of Anderson localization, the exponentially localized envelope, is seen upon integrating the coincidence map along the $x_1 = x_2$ axis. Also, I demonstrated Anderson localization at the single photon level.

In the third paper [15], which is pre-press, I expanded significantly upon the second paper. I again verified the phenomenon of Anderson co-localization, but for more extended input states. I also revealed and experimentally verified the sister phenomenon of Anderson anti-localization, in which an initially anti-correlated input state traverses a disordered array and emerges with its correlations intact. In this report, I exercise control over the correlations at the input by altering the input optical configuration. The correlated state is generated by an imaging system, and the anti-correlated state is generated by a Fourier transforming system. There is of course, a continuum of optical systems between these two extremes; these systems may be described by the fractional Fourier transform. I use these intermediate optical systems to generate two-photon states in which entanglement is not expressed strictly in position, but through a combination of position and phase. I couple these states into the disordered photonic waveguide arrays and show a transition from a correlated state leading to Anderson co-localization to an anti-correlated state leading to Anderson anti-localization.

In the final paper [65], I perform experiments using classical light that explore the action of the

periodic and disordered photonic waveguide arrays in terms of spatial frequency. While many experiments have examined the arrays in terms of their spatial impulse response functions, little work has been done to show the effect on spatial frequency. In this paper, I illustrate the effect of periodic and disordered arrays on four impulse response functions: those that related spatial coordinate or spatial frequency at the input to spatial coordinate or spatial frequency at the output. I also experimentally measure three out of the four impulse response functions for each array. In the periodic array, I show the surprisingly intricate structure of the impulse response function that relates a spatial impulse input to a spatial frequency output. In the disordered array, I reveal the unexpected X-shape present in the impulse response function relating a spatial frequency input to the spatial frequency output. This shape indicates that a plane wave input in the disordered array is not obscured by the disorder as might be expected, but is instead separated into ”reflected” and ”transmitted” components.

The research I have performed and reviewed here has advanced the sciences of discrete optical systems, particularly at the boundary of quantum and discrete optics. These advancements will ideally lead to further research on extended, entangled quantum states in other types of discrete optical systems. Also, my research on impulse response functions in terms of spatial frequency will hopefully lead other researchers to consider the spatial frequency domain in the search for new and interesting physics in novel types of photonic lattices.

APPENDIX : COPYRIGHT PERMISSIONS

The papers from Chapters 2 and 3 were published prior to this dissertation and require release of copyright to be used here. The paper from Chapter 2, ”Anderson localization in optical waveguide arrays with off-diagonal coupling disorder” was published in Optics Express, and permission was granted to reproduce the material as shown in the email and reply below. The second paper, ”Einstein-Podolsky-Rosen Spatial Entanglement in Ordered and Anderson Photonic Lattices” was published in Physical Review Letters, a journal of the American Physical Society. Their policy is explicitly stated on the following website: ”https://journals.aps.org/copyrightFAQ.html”, and allows the use of my work for this dissertation.

Dear Lane Martin,

Thank you for contacting The Optical Society.

Because you are the author of the source paper from which you wish to reproduce material, OSA considers your requested use of its copyrighted materials to be permissible within the author rights granted in the Copyright Transfer Agreement submitted by the requester on acceptance for publication of his/her manuscript. It is requested that a complete citation of the original material be included in any publication. This permission assumes that the material was not reproduced from another source when published in the original publication.

Please let me know if you have any questions.

Kind Regards,

Susannah Lehman

Susannah Lehman August 26, 2014 Authorized Agent, The Optical Society

From: Lane Martin [mailto:lanem@creol.ucf.edu] Sent: Tuesday, August 26, 2014 11:59 AM To: pubscopyright Subject: Copyright Permission for Inclusion of Opt. Exp. Paper in Dissertation

Dear Editor:

I am completing my doctoral dissertation at CREOL, the College of Optics and Photonics at the University of Central Florida. I would like your permission to reprint in my dissertation the following publication, of which I am a co-author:

Anderson localization in optical waveguide arrays with off-diagonal coupling disorder Optics Express, Vol. 19, Issue 14, pp. 13636-13646 (2011) http://dx.doi.org/10.1364/OE.19.013636

The requested permission extends to any future revisions and editions of my dissertation, including non-exclusive world rights in all languages. These rights will in no way restrict republication of the material in any other form by you or others authorized by you. Your granted permission will also confirm that Optics Express owns the copyright to the above-described material.

If these arrangements meet with your approval, please reply to this email granting permission to reprint this work. Thank you for your attention in this matter.

Sincerely,

Lane A. Martin CREOL - The College of Optics and Photonics University of Central Florida

LIST OF REFERENCES

[1] A. Einstein, B. Podolsky, and N. Rosen, Phys. Rev. **47**, 777 (1935).

[2] J. S. Bell, Physics **1**, 195 (1964).

[3] R. Horodecki, P. Horodecki, M. Horodecki, and K. Horodecki, Rev. Mod. Phys. **81**, 865 (2009).

[4] C. H. Bennett and G. Brassard, in *Proceedings of IEEE International Conference on Computers, Systems and Signal Processing*, Vol. 175 (New York, 1984) Chap. 0.

[5] P. W. Shor and J. Preskill, Phys. Rev. Lett. **85**, 441 (2000).

[6] M. A. Nielsen and I. L. Chuang, *Quantum Computation and Quantum Information* (Cambridge university press, 2010).

[7] H. D. Raedt, A. Lagendijk, and P. de Vries, Phys. Rev. Lett. **62**, 47 (1989).

[8] M. Segev, Y. Silberberg, and D. N. Christodoulides, Nature Photonics **7**, 197 (2013).

[9] L. Martin, G. D. Giuseppe, A. Perez-Leija, R. Keil, F. Dreisow, M. Heinrich, S. Nolte, A. Szameit, A. F. Abouraddy, D. N. Christodoulides, and B. E. A. Saleh, Opt.Express **19**, 13636 (2011).

[10] A. Lagendijk, B. van Tiggelen, and D. S. Wiersma, Phys. Today **62**, 24 (2009).

[11] Y. Lahini, A. Avidan, F. Pozzi, M. Sorel, R. Morandotti, D. N. Christodoulides, and Y. Silberberg, Phys. Rev. Lett. **100**, 013906 (2008).

[12] T. Schwartz, G. Bartal, S. Fishman, and M. Segev, Nature **446**, 52 (2007).

[13] P. W. Anderson, Phys. Rev. **109**, 1492 (1958).

[14] G. D. Giuseppe, L. Martin, A. Perez-Leija, R. Keil, F. Dreisow, S. Nolte, A. Szameit, A. F. Abouraddy, D. N. Christodoulides, and B. E. A. Saleh, Phys. Rev. Lett. **110**, 150503 (2013).

[15] L. Martin, G. D. Giuseppe, A. Perez-Leija, R. Keil, S. Nolte, A. Szameit, A. F. Abouraddy, D. N. Christodoulides, and B. E. A. Saleh, "Anderson co-localization to anti-localization of entangled photon pairs in disordered photonic lattices," ().

[16] C. M. Soukoulis and E. N. Economou, Phys. Rev. B **24**, 5698 (1981).

[17] P. Erds and R. Herndon, Adv.Phys. **31**, 65 (1982).

[18] D. N. Christodoulides, F. Lederer, and Y. Silberberg, Nature **424**, 817 (2003).

[19] R. Morandotti, U. Peschel, J. S. Aitchison, H. S. Eisenberg, and Y. Silberberg, Phys. Rev. Lett. **83**, 4756 (1999).

[20] T. Pertsch, P. Dannberg, W. Elflein, A. Bruer, and F. Lederer, Phys. Rev. Lett. **83**, 4752 (1999).

[21] H. Trompeter, W. Krolikowski, D. N. Neshev, A. S. Desyatnikov, A. A. Sukhorukov, Y. S. Kivshar, T. Pertsch, U. Peschel, and F. Lederer, Phys. Rev. Lett. **96**, 053903 (2006).

[22] H. B. Perets, Y. Lahini, F. Pozzi, M. Sorel, R. Morandotti, and Y. Silberberg, Phys. Rev. Lett. **100**, 170506 (2008).

[23] S. Longhi, M. Marangoni, M. Lobino, R. Ramponi, P. Laporta, E. Cianci, and V. Foglietti, Phys. Rev. Lett. **96**, 243901 (2006).

[24] K. Shandarova, C. E. Rter, D. Kip, K. G. Makris, D. N. Christodoulides, O. Peleg, and M. Segev, Phys. Rev. Lett. **102**, 123905 (2009).

[25] A. Perez-Leija, H. Moya-Cessa, A. Szameit, and D. N. Christodoulides, Opt.Lett. **35**, 2409 (2010).

[26] A. Szameit, Y. Kartashov, P. Zeil, F. Dreisow, M. Heinrich, R. Keil, S. Nolte, A. Tunnermann, V. Vysloukh, and L. Torner, Opt.Lett. **35**, 1172 (2010).

[27] Y. Lahini, Y. Bromberg, Y. Shechtman, A. Szameit, D. N. Christodoulides, R. Morandotti, and Y. Silberberg, Phys. Rev. A **84**, 041806 (2011).

[28] J. B. Pendry, Jo. of Phys. C **15**, 5773 (1982).

[29] A. Szameit, F. Dreisow, T. Schreiber, S. Nolte, and A. Tnnermann, Opt. Exp. **14**, 2151 (2006).

[30] A. Szameit, F. Dreisow, T. Pertsch, S. Nolte, and A. Tunnermann, Opt.Express **15**, 1579 (2007).

[31] F. M. Izrailev, T. Kottos, A. Politi, and G. P. Tsironis, Phys. Rev. E **55**, 4951 (1997).

[32] R. Folman, P. Kruger, J. Schmiedmayer, J. Denschlag, and C. Henkel, Adv.At., Mol., Opt.Phys. **48**, 263 (2002).

[33] J. T. Merrill, C. Volin, D. Landgren, J. M. Amini, K. Wright, S. C. Doret, C. Pai, H. Hayden, T. Killian, and D. Faircloth, New Journal of Physics **13**, 103005 (2011).

[34] J. Majer, J. Chow, J. Gambetta, J. Koch, B. Johnson, J. Schreier, L. Frunzio, D. Schuster, A. Houck, and A. Wallraff, Nature **449**, 443 (2007).

[35] A. Politi, M. J. Cryan, J. G. Rarity, S. Yu, and J. L. O'Brien, Science **320**, 646 (2008).

[36] D. Bouwmeester, A. K. Ekert, and A. Zeilinger, *The physics of quantum information: quantum cryptography, quantum teleportation, quantum computation* (Springer Publishing Company, Incorporated, 2010).

[37] E. Knill, R. Laflamme, and G. J. Milburn, Nature **409**, 46 (2001).

[38] Y. Aharonov, L. Davidovich, and N. Zagury, Phys. Rev. A **48**, 1687 (1993).

[39] L. Sansoni, F. Sciarrino, G. Vallone, P. Mataloni, A. Crespi, R. Ramponi, and R. Osellame, Phys. Rev. Lett. **105**, 200503 (2010).

[40] A. F. Abouraddy, M. Nasr, B. E. Saleh, A. V. Sergienko, and M. C. Teich, Physical Review A **63**, 063803 (2001).

[41] C. K. Law and J. H. Eberly, Phys. Rev. Lett. **92**, 127903 (2004).

[42] A. C. Dada, J. Leach, G. S. Buller, M. J. Padgett, and E. Andersson, Nature Physics **7**, 677 (2011).

[43] J. L. O'Brien, A. Furusawa, and J. Vukovi, Nature Photonics **3**, 687 (2009).

[44] Y. Bromberg, Y. Lahini, R. Morandotti, and Y. Silberberg, Phys. Rev. Lett. **102**, 253904 (2009).

[45] C. Hong, Z. Ou, and L. Mandel, Phys. Rev. Lett. **59**, 2044 (1987).

[46] Y. Lahini, Y. Bromberg, D. N. Christodoulides, and Y. Silberberg, Phys. Rev. Lett. **105**, 163905 (2010).

[47] A. F. Abouraddy, G. D. Giuseppe, D. N. Christodoulides, and B. E. A. Saleh, Phys. Rev. A **86**, 040302 (2012).

[48] R. J. Glauber, Phys.Rev. **130**, 2529 (1963).

[49] T. Yarnall, A. F. Abouraddy, B. E. Saleh, and M. C. Teich, Phys. Rev. Lett. **99**, 170408 (2007).

[50] A. Peruzzo, M. Lobino, J. C. Matthews, N. Matsuda, A. Politi, K. Poulios, X.-Q. Zhou, Y. Lahini, N. Ismail, K. Worhoff, *et al.*, Science **329**, 1500 (2010).

[51] A. Schreiber, A. Gabris, P. P. Rohde, K. Laiho, M. Stefanak, V. Potovcek, C. Hamilton, I. Jex, and C. Silberhorn, Science **336**, 55 (2012).

[52] P. Shadbolt, M. Verde, A. Peruzzo, A. Politi, A. Laing, M. Lobino, J. Matthews, M. Thompson, and J. O'Brien, Nature Photonics **6**, 45 (2011).

[53] C. H. Bennett, G. Brassard, C. Crpeau, R. Jozsa, A. Peres, and W. K. Wootters, Phys. Rev. Lett. **70**, 1895 (1993).

[54] D. Bouwmeester, J.-W. Pan, K. Mattle, M. Eibl, H. Weinfurter, and A. Zeilinger, Nature **390**, 575 (1997).

[55] K. W. Chan, J. P. Torres, and J. H. Eberly, Phys. Rev. A **75**, 050101 (2007).

[56] D. S. Tasca, S. P. Walborn, P. H. S. Ribeiro, and F. Toscano, Phys. Rev. A **78**, 010304 (2008).

[57] D. S. Tasca, S. P. Walborn, P. H. S. Ribeiro, F. Toscano, and P. Pellat-Finet, Phys. Rev. A **79**, 033801 (2009).

[58] S. Perseguers, M. Lewenstein, A. Acn, and J. Cirac, Nature Physics **6**, 539 (2010).

[59] J. R. Ott, N. Mortensen, and P. Lodahl, Phys. Rev. Lett. **105**, 090501 (2010).

[60] A. Crespi, R. Osellame, R. Ramponi, V. Giovannetti, R. Fazio, L. Sansoni, F. D. Nicola, F. Sciarrino, and P. Mataloni, Nature Photonics (2013).

[61] D. Mendlovic and H. M. Ozaktas, JOSA A **10**, 1875 (1993).

[62] H. M. Ozaktas and D. Mendlovic, JOSA A **10**, 2522 (1993).

[63] A. F. Abouraddy, B. E. A. Saleh, A. V. Sergienko, and M. C. Teich, JOSA B **19**, 1174 (2002).

[64] B. E. A. Saleh, A. F. Abouraddy, A. V. Sergienko, and M. C. Teich, Phys. Rev. A **62**, 043816 (2000).

[65] L. Martin, R. Keil, S. Nolte, A. Szameit, A. F. Abouraddy, and B. E. A. Saleh, "Spatial frequency in periodic and anderson disordered photonic lattices," ().

[66] S. Longhi, Laser Photon. Rev. **3**, 243 (2009).

[67] T. Pertsch, T. Zentgraf, U. Peschel, A. Br, and F. Lederer, Phys.Rev.Lett. **88**, 093901 (2002).